Fluorescence Recovery After Photobleaching of Rapsyn-EGFP in the Neuromuscular Junction of Mice In Vivo.

Catherine E. Sem-Jacobsen

A thesis submitted for the degree of Master of Science

Department of Molecular Biosciences
Faculty of Mathematics and Natural Sciences
The University of Oslo
Fall of 2005

ACKNOWLEDGEMENTS

This project was conducted at the Department of Molecular Biosciences in the physiology program under the guidance of Kristian Gundersens, during 2004 and 2005.

First of all I want to thank Kristian for being so interested in my work and for wanting everything to be perfect. I also want to thank Jo, for teaching me all the tricks in the book on how to do research with animals and for introducing me to the world of graphs and macs.

Many thanks to Bill Philips at the University of Sydney, for supplying the rapsyn-EGFP plasmid and for taking the time to read and give crucial comments on my results and thesis as a whole.

Thanks to Kristin for valuable help and I wish her good luck on continuing the project. Thanks also to the rest of the muscle group and the physiology program for making this a good experience. Thanks to my two proofreaders John and Joan.

All my family and friends deserve a thousand thanks for listening to my whining and complaining about how much work I have to do and about the stupid mouse that died and so on for the last two years, especially Rolf, thank you!

Oslo, September 2005

Catherine Sem-Jacobsen

ABSTRACT

The high densities of receptors found in synapses are crucial for effective transmission between a nerve and its target cell. At the neuromuscular junctions, acetylcholine is the transmitter substance and its receptor, the acetylcholine receptor (AChR) is found at very high concentrations in the endplate on the postsynaptic membrane. A large array of molecules is necessary to form the clusters of AChR during development and to keep up the highly structured arrangement of the endplate. One of these molecules is rapsyn. Rapsyn is a peripheral membrane protein. It has binding sites for several of the proteins in the endplate and is closely associated with the AChR. Without this protein's presence no endplate structures form. Rapsyn can also induce clustering of AChR in several non-muscle cell lines when cotransfected with the subunits of the receptor.

In this project a plasmid containing rapsyn tagged with the enhanced green fluorescent protein (EGFP) was electroporated into the *extensor digitorum longu* (*edl*) muscle of mice. The resultant rapsyn-EGFP chimera localises to the endplate in exchange for and in addition to, wild type rapsyn. With the argon laser of a confocal microscope a portion of the rapsyn-EGFP in the endplates was photobleached. The subsequent fluorescent recovery was studied using a fluorescent microscope with a SIT camera. The hypothesis was that the recovery of rapsyn-EGFP would mimic the recovery seen when bleaching labelled AChR in the endplate consistent with the idea that rapsyn forms a complex with AChR already before clustering

Contrary to our expectations, we found that rapsyn-EGFP had a recovery rate, after photobleaching, which was about 14-68-fold higher than that established for the AChR. There seemed to be two pools of rapsyn-EGFP in the endplates with a fast recovering pool constituting about 60-80% of the endplate population and a non-recovered portion consisting of the remaining 20-40% of the endplate population. The recovering pool had a higher turnover and/or mobility than the receptor leading us to suppose that such molecules are either not associated with receptors, or associated with receptors for only shorter periods of time. Furthermore, it is possible to suppose that the non-recovered pool act as complexes with receptors throughout their lifetime, or these might also associate and disassociate with receptors.

TABLE OF CONTENTS

1 INTRODUCTION

1.1 Morphology of the neuromuscular junction

The neuromuscular junction has been widely used for studying the different aspects of the synapse; this is mainly because of its large size and easy accessibility, as well as its simplicity in the fact that only one motor axon innervates a fibre. There is one single synapse on each muscle fibre. There are four main components of the neuromuscular junction; 1) the presynaptic cell with its nerve terminal, 2) the postsynaptic muscle fibre, 3) the synaptic cleft filled by the basal lamina and 4) the Schwann cell that covers the nerve terminal (Fig. 1.1).

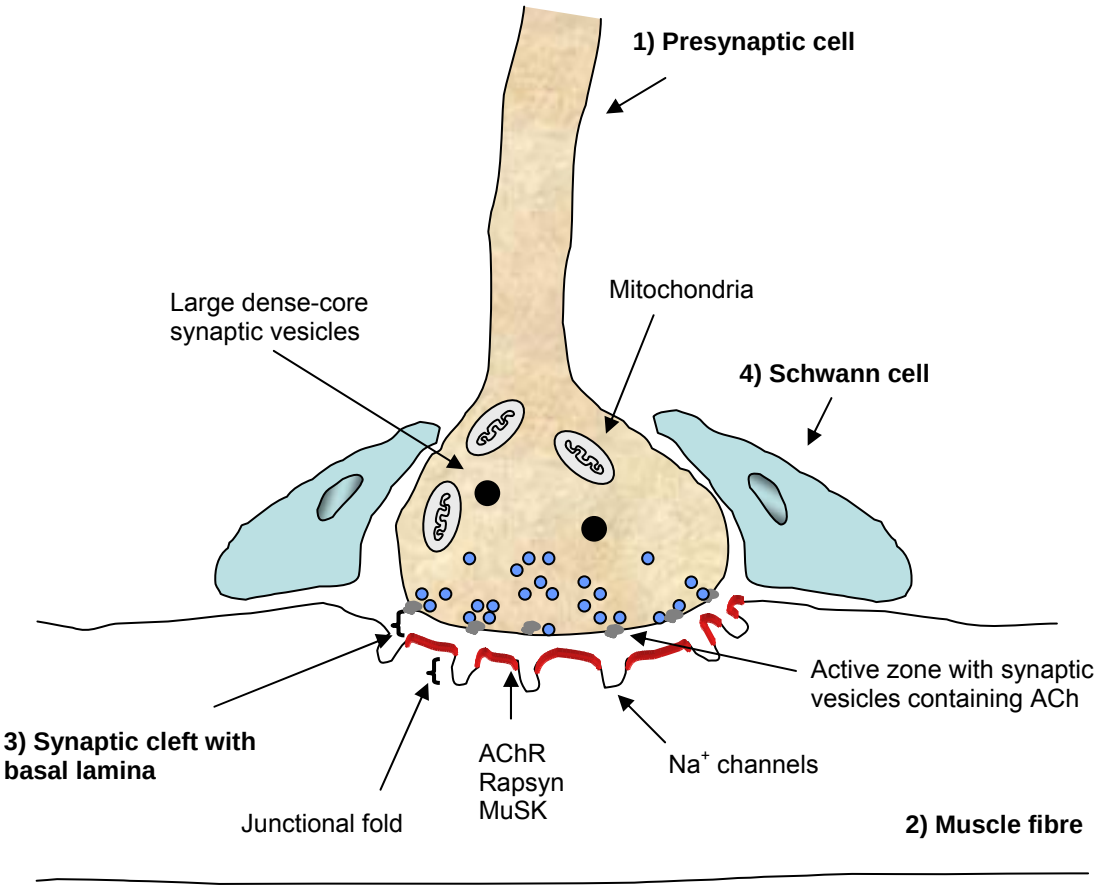

Figure 1.1 Morphology of the synapse. 1) A branch of a motor nerve axon reaches a muscle fibre and divides. Each of these small branches terminates in boutons that make up the nerve terminal. The bouton contains mitochondria and numerous synaptic vesicles with the neurotransmitter acetylcholine (ACh). 2) Postsynaptically, the muscle fibre membrane is folded. Acetylcholine receptors (AChR) are concentrated on top of the junctional folds along with structurally important proteins (indicated in red). Voltage-gated sodium channels are found on the bottom of the folds. 3) Between the pre- and postsynaptic cells is the synaptic cleft, filled with specialised basal lamina. 4) Shwann cells cover the junction.

The axon of the motor nerve branch intramuscularly to innervate multiple muscle fibres. On each fibre the axon again divides and terminates in a spray of boutons (Hall & Sanes, 1993). Each bouton of the nerve terminal is filled with small synaptic vesicles. There are also so-called, large dense-core vesicles which make up 1 % of the total vesicle-population (Cowan *et al.*, 2001).

The small synaptic vesicles are filled with the neurotransmitter Acetylcholine (ACh) and have a diameter of 50 nm (Hall & Sanes, 1993). They are assembled in clusters close to the active zones in the plasma membrane facing the synaptic cleft, where some vesicles are docked and ready for fusion and transmitter release. The active zones are the only sites at which docking and fusion of the small synaptic vesicle occurs.

The large dense-core vesicles are so called because of the dark core seen in the electron microscope. These have a diameter of 70-200 nm and they contain neurotransmitters, neurohormones and sometimes amines. These are released outside the active zones and normally act via slower systems like G-protein coupled receptors. Their role is probably to modulate the synaptic transmission (Cowan *et al.*, 2001).

Mitochondria are found closely associated with the clusters of small synaptic vesicles. This is because of the large ATP (Adenosine triphosphate) consumption during the vesicle cycle in which the vesicles dock, fuse and undergo endocytocis to make new vesicles that are filled with new ACh molecules (Cowan *et al.*, 2001). The cytosol of the neuron terminal also contains proteins such as Choline acetyltransferase and Choline transporters to ensure new synthesis of ACh (Cowan *et al.*, 2001).

Underneath the membrane with its active zones is the 50 nm wide synaptic cleft (Hall & Sanes, 1993). The cleft is filled with basal lamina, which covers the endplate and protrudes down into folds in the postsynaptic membrane (Hall & Sanes, 1993). This basal lamina contains collagen IV, laminin, entactin and heparin sulphate proteoglycans like that encasing the rest of the muscle fibre but with different isoforms (Sanes & Lichtman, 1999). In addition, basal lamina in the synaptic cleft contains a form of the Aceltylcholinesterase (AChE), a set of glykoconjugates and the two nerve-derived signal molecules, neural agrin and neuregulin (Sanes & Lichtman, 1999).

These proteins are synthesised in the motor nerve and transported down to the nerve terminal in large dense core vesicles and are released into the basal lamina. Neuregulin induces selective expression of AChR genes by the specialised synaptic nuclei (Sanes & Lichtman, 1999). Agrin binds laminin in the basal lamina and thereby reaches high concentrations (Ruegg & Bixby, 1998). This protein will be discussed further in the next section.

The endplate on the muscle fibre surface is slightly invaginated into a shallow gutter. This is further folded into 1μm deep grooves. The acetylcholine receptor (AChR) is concentrated at >10,000/μm^2 on the tops of these folds and is also found a short way down the sides (Hall & Sanes, 1993; Sanes & Lichtman, 1999). There is a close association between the structure of the pre- and postsynaptic sites with the active zones opposite the junctional grooves and close to the receptors (Hall & Sanes, 1993).

The membrane of the postsynaptic cell forms the specialised structure of the endplate packed with an array of different proteins important for the structural organisation of the endplate and the connection with the presynaptic cells. Integrin, N-CAM and ankyrin, are important for connecting the cytoskeleton of the cell via the membrane and basal lamina to the presynaptic cell (Hall & Sanes, 1993). At the top of the folds associated with the receptor is rapsyn, a peripheral membrane protein, and the muscle specific kinase MuSK, as well as other structural proteins such as β-dystroglycan utrophin, α-dystrobrevin-1 and syntrophin (Sanes & Lichtman, 1999). Voltage-gated sodium channels are concentrated at the bottom of the folds along several special synaptic proteins (Sanes & Lichtman, 1999).

Right underneath the bottom of the junctional grooves are specialised synaptic nuclei that are important in transcribing the genes for all the special postsynaptic proteins (Hall & Sanes, 1993). Schwann cells make up myelin sheaths around the axons but they also cap the nerve terminal. They protect the nerve against chemical and mechanical stress (Hall & Sanes, 1993) and are important in clearing away neurotransmitters to end the response, for shielding synapses from each other and to ensure the spatial specificity (Cowan *et al.*, 2001). They sense the electric signals in the nerve and respond with a calcium transient and upon denervation they synthesis and release ACh (Hall & Sanes, 1993).

1.2 AChR, mobility and turnover

A large difference in the mobility of AChR in the endplate and in extra-junctional regions was discovered early in the 1970s. Berg and Hall (1974) found a four times larger reduction over a 24 hour period in labelling for AChR extra-synaptically than synaptically.

AChRs in the membrane of muscle cells were subsequently divided into two pools, the junctional immobile pool and the extra-junctional mobile pool (Axelrod *et al.*, 1976b). Later it was discovered that all AChRs are more or less mobile there are not two distinct pools, but a continuing exchange of AChR between synaptic and extra-synaptic regions. The difference lies in how long the receptor stays in the different regions (Akaaboune *et al.*, 1999; Akaaboune *et al.*, 2002).

The receptor has a half-life of 9 to 14 days (Steinbach *et al.*, 1979; Akaaboune *et al.*, 1999; Akaaboune *et al.*, 2002), but this is not constant during development and before the first postnatal week the receptor half-life is only 1 day (Wang *et al.*, 1999). After the change occurs from short to long half-life, there is also a change in the subunits comprising the receptor. The γ subunit is exchanged with a ε subunit to give the adult combination of subunits, $\alpha_2\beta\varepsilon\delta$. This leads to changes in channel properties with a shorter opening time, but is not necessary for the change in half-life (Hall & Sanes, 1993).

The mobility for AChR outside the endplate is similar to that of diffusely distributed AChR in cultured myotubes (Stya & Axelrod, 1983, 1984; Kuromi *et al.*, 1985; Velez *et al.*, 1990). AChR in extra-junctional clusters in cell culture have a lower mobility, while the junctional receptors are even lower (Stya & Axelrod, 1984). In the synaptic endplate an AChR is maintained in one spot for about 8 hours (Akaaboune *et al.*, 2002). They move around slowly and within 4 days one will have crossed the whole endplate, migrating either directly or via the perisynaptic region. Receptors from the extra-synaptic space move into the endplate and contribute to keeping a high density of receptors in the endplate (Akaaboune *et al.*, 2002).

Most of these studies have been performed by using the Fluorescent Recovery After Photo-bleaching (FRAP) technique in which a small spot is bleached with a high intensity laser and the subsequent recovery is measured over an appropriate time range (further described in 2.4).

Stya and Axelrod (1983) combined this method with the detergent extractability method and found that the cytoskeletal framework is likely to be involved in the immobilization of AChRs at the endplate. The cytoskeleton is likely to work by trapping and stabilising receptors (Heuser & Salpeter, 1979; Hirokawa & Heuser, 1982; Bloch & Hall, 1983; Peng, 1983; Velez *et al.*, 1990).

As mentioned earlier in this chapter, the nerve continuously releases agrin, which accumulates in the basal lamina. Agrin was for a long time considered the initiator of postsynaptic differentiation and AChR clustering (Ruegg & Bixby, 1998). MuSK is the downstream effecter of agrin and is a part of the receptor for neural agrin (Sander *et al.*, 2001) but MuSK cannot bind the AChR by itself (Ruegg & Bixby, 1998; Sanes & Lichtman, 1999). Upon agrin signalling, in the presence of rapsyn, MuSK is phosphorylated which then further leads to the phosphorylation of the β-subunit of the AChR (Ruegg & Bixby, 1998). However rapsyn can also through autophosphorylation activate MuSK without agrin. The same AChR phosphorylation is obtained and the receptors are clustered (Gillespie *et al.*, 1996). Rapsyn is therefore a probable link between the receptor and the cytoskeleton.

1.3 Rapsyn

Rapsyn is a 43 kD receptor-associated protein earlier known as the “43 kD protein”. The term rapsyn is short for Receptor Associated Protein at the SYNapse (Frail *et al.*, 1988). The primary structure of the protein is well known and mutational analyses have given the function of the different domains (Fig. 1.2). The N-terminal contains a glycin, which is myristoylated (Frail *et al.*, 1988). Then there are 8 tetracopeptide repeats (TPRs) (Freemont, 1993), a coiled-coil domain (Ramarao & Cohen, 1998) a cystein rich domain, predicted to be a RING-H2 domain (Ponting & Phillips, 1996) and a short consensus sequence for phosphorylation by proteinkinase A and C and finally the C-terminal (Bartoli *et al.*, 2001).

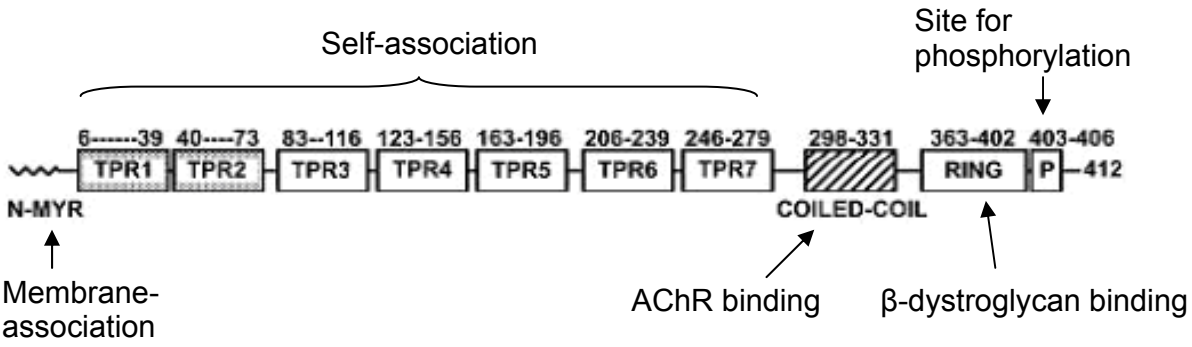

Figure 1.2 The structural domains of rapsyn modified from Ramarao et al. 2001. The N-terminal myristoylation is important for membrane association (Phillips *et al.*, 1991b). Different combinations of the TPRs give self-association while the coiled-coil is responsible for binding to the receptor (Ramarao *et al.*, 2001). The RING-H2 domain binds to β-dystroglycan (Bartoli *et al.*, 2001), which is a membrane protein (se Fig. 1.3) and C terminally there is a phosphorylation site (Frail *et al.*, 1987).

Rapsyn was isolated by Sobel and co-workers while purifying and characterising the AChR from the electric organ membrane of *Torpedo marmorata* (Sobel & Changeux, 1977; Sobel *et al.*, 1977a; Sobel *et al.*, 1977b). Frail et al. (1987) cloned rapsyn cDNAs from the same source. They obtained two similar cDNAs one containing 23 additional amino acids at the C terminus. They also cloned rapsyn cDNA from the mouse where only one rapsyn gene was found in its genome. There is a homology between the two species of 70 %, highly conserved sequence include the C-terminal and the phosphorylation site (Frail *et al.*, 1987).

Neubig et al. (1979) extracted the rapsyn protein from AChR rich membranes by alkalinization (raising the pH to 11). This indicated that rapsyn should be considered a peripheral rather than an integral membrane protein. It was also tested whether rapsyn is in fact a intrinsic component of the receptor-rich membrane and is not just getting trapped within the membrane fragments when these are extracted (Wennogle & Changeux, 1980). Rapsyn is located on the cytoplasmic side of the plasma membrane in the Torpedo electric organ (Sealock, 1982; St John *et al.*, 1982) and also in mammalian muscle endplate (Porter & Froehner, 1983).

Rapsyn is closely co-localised with the AChR (Froehner *et al.*, 1981; Sealock, 1982) and they are both found in approximately equimolar concentrations in the Torpedo electric organ, also in skeletal muscle but have only been detected in minute amounts (<0,1 pmol/mg tissue

protein) in the heart, liver, pancreas and brain. This shows that Rapsyn is not a general membrane or synapse associated protein, but is specific for AChR rich membranes (LaRochelle & Froehner, 1986). Other studies that have been done by rapsyn-extraction show that rapsyn stabilises the receptor against heat inactivation (Saitoh *et al.*, 1979) and decreases the rotational (Rousselet *et al.*, 1982) and lateral (Barrantes *et al.*, 1980) diffusion of the receptor. Rapsyn also reduces the triton X-100 extractability of the receptor (Phillips *et al.*, 1993). These findings indicate rapsyn's function as closely linked to the receptor.

Rapsyn exists in a stoichometry of approximately 1:1 with the AChR (Sobel *et al.*, 1978; Sealock, 1982; LaRochelle & Froehner, 1986; Apel *et al.*, 1995). Burden et al. (1983) showed that these two proteins can be cross linked and that they are in close proximity of each other. The expression of rapsyn is however not liked to that of the receptor (Frail *et al.*, 1989). While AChRs are not expressed in undifferentiated muscle cells, rapsyn is and though the concentration of AChRs varies greatly through development, rapsyn expression stays close to constant (Frail *et al.*, 1989). Frail et al. (1989) also found a large difference in the degradation kinetics of the two proteins. While the receptor has a half-life of up to 14 days in the neuromuscular junction (Akaaboune *et al.*, 1999), in cultured C2 cells it is only about 8 hours. Rapsyn has a half-life in these cells of only 2.4 hours (Frail *et al.*, 1989). This indicates that rapsyn might also have a shorter half-life in the endplate than that of the receptor.

1.3.2 Funcion

During formation of the neuromuscular junction the AChRs start clustering together already before the muscle cells are contacted by the nerve (Sanes & Lichtman, 1999). Cultured muscle cells also show these spontaneously occurring clusters of AChR (Anderson & Cohen, 1977). After the muscle has been innervated new clusters are formed at the site of innervation and in mice, a fully functional synapse is formed within one week (Sanes & Lichtman, 1999).

The quail fibroblast cell line expresses no endogenous AChR. Transfecting these cells with the four subunits of fetal or adult AChR resulted in the receptor being dispersed on the surface of the cells. When these cells were transfected with mouse rapsyn as well, they showed

clustered AChR co-localized with rapsyn aggregates, similar to the clusters in muscle cells. Rapsyn was also able to form clusters without AChR or neural agrin being present (Phillips *et al.*, 1991a). Similar results were obtained when the experiment was done in Xenopus oocytes (Froehner *et al.*, 1990).

Later studies also done with quail fibroblast show that when rapsyn is cotransfected with the AChR the reseptor is not only clustered but its half-life increases (Phillips *et al.*, 1997). Gautam et al. (1995) confirmed that rapsyn is essential for AChR clustering by constructing rapsyn-deficient mice. These mice had severely affected neuromuscular function and died shortly after birth. Unlike each fibre of normal muscle, the diaphragm muscle of the mutated mice contained no AChR clusters anywhere along the fibres (Gautam *et al.*, 1995).

As well as clustering the receptor, rapsyn clusters β-dystroglycan, both with and without AChRs present in the clusters (Apel *et al.*, 1995), and the muscle specific kinase MuSK (Gillespie *et al.*, 1996). β-dystroglycan is a component of the dystrophin-glycoprotein complex (DGC) which functions as a link between the extracellular matrix and the internal cytoskeleton (Apel *et al.*, 1995), Fig. 1.3. As seen from Fig. 1.2, rapsyn has a binding site for β-dystroglycan. This may be the link between rapsyn and the cytoskeleton and thus the two proteins mechanically support and stabilise the receptor (Apel *et al.*, 1995).

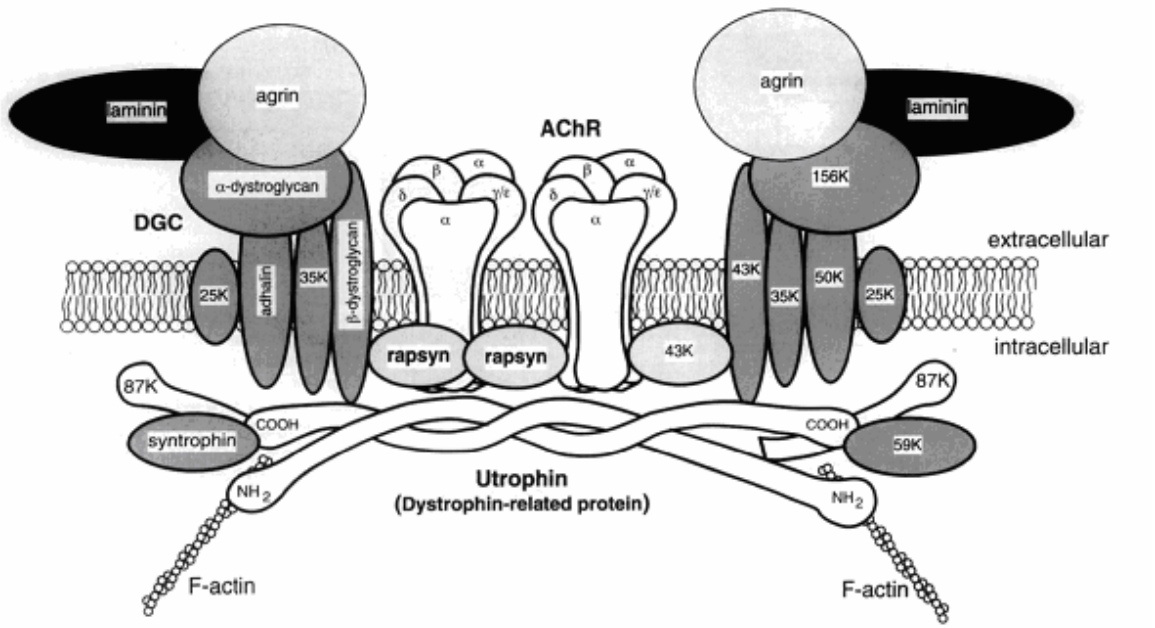

Figure 1.3 Schematic Model of the Hypothetical Molecular Organization of the Post-synaptic Apparatus at the Neuromuscular Junction from Apel et al. 1995. Molecules proposed to play a role in AChR clustering at the neuromuscular junction arranged with predicted interactions are shown. Molecular weights corresponding to the names on the left are shown on the right. Rapsyn binds to the receptor in clusters. It is suggested that rapsyn links the AChR to the DGC, thereby facilitating the association of AChR clusters with the cytoskeleton.

As well as functioning as a direct link between the receptor and the cytoskeleton, rapsyn also plays an important chemical role thorough phosphorylation (Mohamed & Swope, 1999). Rapsyn itself does not have a kinase domain (Frail *et al.*, 1987) and cannot therefore phosphorylate any proteins, but it has the capability of activating Src kinases. The subsequent phosphorylation of AChRs induce translocation and anchoring of these to the cytoskeleton and following stabilisation (Mohamed & Swope, 1999).

1.3.3 Rapsyn AChR binding

Each of the five AChR subunit can be clustered by rapsyn individually (Maimone & Merlie, 1993). The major cytoplasmic loop of the subunits contains the rapsyn binding site. Each receptor can therefore bind up to five rapsyn molecules (Huebsch & Maimone, 2003). Normally however, only one or two rapsyn molecules are bound to each AChR (Burden *et al.*, 1983; LaRochelle & Froehner, 1986; Miyazawa *et al.*, 1999).

When overexpressing rapsyn as a rapsyn-EGFP chimera, the molecule occupies available sites on the AChR (Gervasio & Phillips, 2005). The Rapsyn-to-AChR ratio increases and the density of rapsyn increases 1.8-fold. This increased ratio of Rapsyn to AChR further stabilizes postsynaptic receptors by reducing its half-life, but there is no increase in AChR number (Gervasio & Phillips, 2005).

Wang et al. (1999) also showed that rapsyn stabilises the receptor by interacting with it. The stabilising effect is independent of the clustering function, even though both functions are dependent on the same domains of rapsyn. Herbimycin A, which blocks clustering, has no effect on the half-life of the receptor, and the metabolic stabilization is not affected by cytoskeletal disrupting agents. On the other hand when mutating the domains necessary for clustering, both the clustering process and the effect on AChR turnover, are severely reduced (Wang *et al.*, 1999). These clustering independent stabilising effects are likely to be associated with the Src kinases mentioned earlier.

Furthermore they suggest that both the AChRs that are un-clustered and those in clusters are associated with rapsyn (Wang *et al.*, 1999). This is also indicated by the fact that AChR and rapsyn co-distribute within the distal exocytotic routes and are therefore probably inserted into the membrane as a complex (Marchand *et al.*, 2002). It is likely that the AChR and rapsyn diffuse laterally within the membrane as a complex. Rapsyn should therefore have a similar mobility to that of the receptor.

This view is supported by the findings of Gervasio and Phillips (2005) who discovered a similar half recovery time with FRAP for the receptor and rapsyn in the cytosol of C2 myotubes. Also, as with the receptor, rapsyn had no detectable recovery after photobleaching on muscle fibre endplates over a 20 min period (Gervasio & Phillips, 2005).

1.4 Aims

The aim of this study has been to investigate the recovery after photobleaching of rapsyn and the half recovery time for this process, in vivo in the neuromuscular endplate of mice over a longer time period. A second aim was the investigation of how rapsyn moves around in the endplate of the muscle fibre

Hypotheses

- Rapsyn and the AChR diffuse laterally as a complex within the plasma membrane consistent with the idea that rapsyn assembles with AChR in the exocytic pathway. Rapsyns recovery after photobleaching should therefore be similar to that for the AChR.

- The receptors move around within the endplate and via the perisynaptic region and a high density is maintained by receptors migrating in from the surroundings. If rapsyn acts as a complex with the receptor, the recovery after photobleaching should be caused by rapsyn-EGFP moving in to the endplate as well as movement within the endplate.

2 MATERIALS AND METHODS

2.1 Animal experiments

The animal experiments were conducted in accordance with the Norwegian Animal Welfare Act of 20 December 1974 (no. 37, chapter VI, sections 20-22) and approved by the Norwegian Animal Research Authority.

Female NMRI mice (20-35g) were held in cages in the animal facilities of the Department of Molecular Biosciences at the University of Oslo.

The mice were anesthetised by intraperitoneal injection of 5µl (g body weight)$^{-1}$ Equthesin (Ullevål Sykehus, Norway, Pnr.: 502854, 42.5 mg of chloral hydrate and 9.7 mg pentobarbitone per ml, appendix B). The depth of the anaesthesia was controlled by regularly pinching the mouse in the metatarsus region to check the withdrawal reflex and more Equthesin was administered when necessary.

Hair on the right leg was shaved off and remaining hair removed with a hair-removing cream (Veet, Reckitt Benckiser). The cream was cleaned off with water and the skin disinfected with 70% ethanol. The skin and facia were cut open on the front of the leg and *musculus tibialis anterior* pulled aside using a small glass rod. This exposes *musculus extensor digitorum longus* (*edl*). The muscle was electroporated (section 2.3) and the cut sewn up (supramid 0,7mm Polyamid thread monofilament, B. Braun Surgical GmbH).

After 6-9 days the mice were again anesthetised and placed on a warming plate designed to fit on the microscope stage. The plate held a temperature of about 35˚C throughout the experiment. After hair removal and disinfection of the skin, a thin layer of vaseline was smeared across the skin as a hydrophobic barrier to avoid the saline solution leaking off from the wound. The leg was then reopened and a suspension of micro spheres (InSpeck^{TM} micro spheres, 6 µm, Green (505/515) fluorescents, with a relative intensity of 1%, Molecular Probes Eugene, USA) and Ringer lactate (appendix B) applied to the muscle. A coverslip attached between two magnets, was placed over the wound to keep the Ringer in place. FRAP

experiments were conducted on endplates of muscle fibres expressing rapsyn-EGFP. The mice were then killed by neck dislocation.

2.2 The Rapsyn-EGFP plasmid

To follow the rapsyn protein in the endplate of *edl*, a plasmid encoding a rapsyn-EGFP fusion protein was used (Fig. 2.1). This was supplied by William D. Philips at the department of Physiology at University of Sydney, Australia (Gervasio & Phillips, 2005). Rapsyn (1,2 kb) was ligated between the BamH1 and EcoRI sites of clonetech pEGFP-N1 plasmid (4,7 kb). This produces a Rapsyn-EGFP chimera (72 kDa) under the transcriptional control of the Cytomegalovirus Immediate early gene (CMV) promoter. The plasmids was purified by Qiagen Maxiprep (Gervasio & Phillips, 2005).

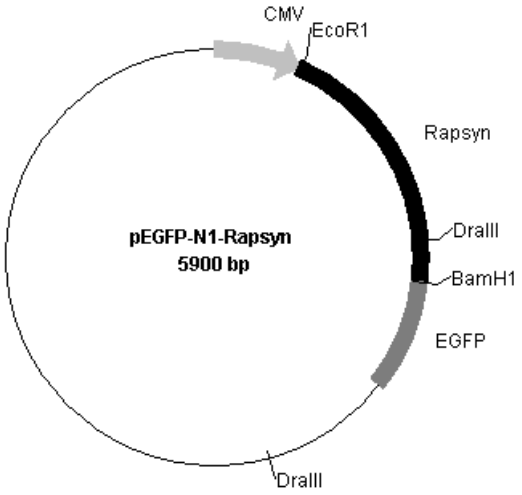

Figure 2.1 pEGFP-N1-Rapsyn plasmid, 5.9 kb.

2.3 Electroporation

Muscle cells have the capability of taking up and expressing DNA in vivo (Wolff *et al.*, 1990). The electrical stimuli applied by electroporation increases the transfection efficiency markedly by membrane permeabilization and increased DNA uptake (Mathiesen, 1999). The method is modified as described previously (Rana *et al.*, 2005).

The exposed muscle was covered with 20-25 µl of the DNA solution (appendices B). An electric field was applied to the muscle with a pulse generator (Pulsar 6bp-a/s, Fredrick & Co). The electrodes consisted of 1 mm thick, 2 cm long silver wires, spaced about 2 mm apart. The wires were placed on either side of the muscle and 5 trains of pulses conducted down the muscle separated by 1 s intervals. Each train consisted of 1000 symmetrical, bipolar, square pulses with duration of 200 µs for each pulse, which gives a frequency of 5 kHz, and with amplitude of 10 Volts in each direction. The electric field was registered with an analogue oscilloscope (03245A, Gould Advance).

2.4 Fluorescence Recovery After Photobleaching (FRAP)

Fluorescence Recovery After Photobleaching (FRAP) is the main method used in this project. It is also known as fluorescence photo bleaching recovery (FPR) technique. The method allows for the analysis of the two-dimensional lateral mobility of fluorescent particles (Axelrod *et al.*, 1976a). If the molecule is mobile in all dimensions the third dimension of depth, will also have an effect on the results gathered. In the case of membrane-bound proteins the third dimension will represent new molecules inserted into the membrane from the cytosol or newly synthesised proteins.

The method has been widely used in studying the lateral mobility of proteins and lipids (Edidin *et al.*, 1976; Jacobson *et al.*, 1976; Schlessinger *et al.*, 1976; Zagyansky & Edidin, 1976; Peng *et al.*, 1989; Gervasio & Phillips, 2005) and of membrane proteins such as the AChR (Axelrod *et al.*, 1976b; Stya & Axelrod, 1983, 1984; Kuromi *et al.*, 1985), as described in the introduction.

Photobleaching is the process where each fluorescent molecule looses its ability to emit fluorescence by undergoing repeated cycles of excitation and emission when exposed to high intensity light (Carrero *et al.*, 2003). All fluorescently labelled proteins, in one spot on the surface of the cell, are photobleached by brief exposure to an intense, focused laser beam. The recovery of the fluorescence is monitored by the same, but attenuated, laser beam or some equivalent light source (Axelrod *et al.*, 1976a).

2.5 Photo-unbinding

Photo-unbinding is a process in which a fluorescently marked ligand dissociates from its receptor as a result of a high-intensity, short duration light-flash. α-bungarotoxin (α-BuT), which can be marked with flurophores, binds to AChR and labels them. When bleaching these on a cell surface, a small portion of the molecules will separate from the receptor. These displaced fluorescent molecules are able to rebind to AChR. The same receptor can undergo multiple unbinding and rebinding cycles (Akaaboune *et al.*, 2002).

The unbinding process is not linearly related to the light intensity. While all intensities cause photobleaching only high intensity light cause photo-unbinding (Akaaboune *et al.*, 2002).

2.6 FRAP on the neuromuscular endplate

When using the FRAP technique one has to be certain that the fluorescently tagged protein under study can substitute functionally for the endogenous protein. Gervasio and Phillips (2005) showed this in three ways. Firstly, myotubes transfected with rapsyn-EGFP show large numbers of tiny AChR-rapsyn-EGFP aggregates in the same way as myotubes transfected with wild-type rapsyn does. Secondly, as observed with wild-type rapsyn, when expressed at low levels in myotubes, rapsyn-EGFP participated in the formation of large AChR clusters in response to neural agrin treatment. Thirdly, Rapsyn-EGFP localises to the endplate in the same way as wild-type rapsyn and this is due to the rapsyn part of the chimera and not the EGFP moiety, which diffusely fills the cytoplasm when expressed alone (Gervasio & Phillips, 2005).

2.6.1 Bleaching

Two sets of experiments were conducted; so called "small" and "large" bleachings. The areas of the "small" (30-80 μm^2) bleachings was of the same order of magnitude as used previously when bleaching endplates (10 μm^2) (Axelrod *et al.*, 1976b), while the "large" bleachings were one order of magnitude larger (800-1600 μm^2) and encompassed a large fraction of the total endplate area. This severely affected the time needed for bleaching. The power of the laser beam was constant 40 mW where it entered the microscope and not proportional to the degree of confocal zooming.

The bleaching was conducted by zooming in on the area to be bleached, increasing the laser to 100% intensity and scanning until the structures in this area were no longer visible. For a large bleaching, the zoom was 4-8x and it took 200-400 scans for complete bleach, up to ten minutes. For a small bleaching the zoom was 20-40x and 20-50 scans (about one minute) was needed.

When zooming, the size of the pixels changes while the time the laser spends on each pixel stays constant (2µs/pixel, in these experiments). Therefore when zooming in and bleaching a small area, a pixel corresponds to a small spot of the endplate, which takes a short time to bleach. When not zooming in as much, the pixel corresponds to a larger area which needs more time to bleach. The time required to bleach the large area was therefore correspondingly longer. The relative photo-load per area is the same for the small and the large but the total photo-load increases linearly with the size of the area.

2.6.2 Micro Spheres as internal controls

As the light source and other components of the microscope system can be unstable over time green fluorescent micro spheres were used as an internal fluorescent standard for each photo. These were applied to the muscle upon reopening (section 2.1) and can then be found scattered over the surface of the muscle. The sphere closest to an endplate was used as control for this endplate.

2.6.3 Taking the photomicrographs

Separate photomicrographs (also referred to as photos or pictures) of each endplate and its corresponding micro sphere were taken before the bleach, directly afterwards and then every 30 min for five hours. The photos were taken by placing the endplate or micro sphere in the centre of the camera-field. For the endplate, the plane that ensured that the area to be bleached was in focus was found, and for the micro sphere, the centre was in focus. A photomicrograph was taken at this focus and then 1µm above and 1µm under this level. Photos were taken after bleaching, in the same way by finding the plane of focus as used in the pre-bleach photo and taking three photos with the z-plane spaced 1µm apart. These 36 (12*3) photos make up one series of one endplate or one micro sphere.

This was done to ensure that photos in a series were as close to each other in focus as possible. When analysing the experiments, the photos that were most similar in focus plane in each time series were selected out of the three taken at each time point and were measured, as described in section 2.9.

2.7 Confocal microscopy

For the experiments, a fluorescence microscope (Olympus BX61WI) with a confocal part (Olympus Fluoview FV 1000) and a 60x water immersion objective (LUMPlan FI, Olympus) was used. The excitation wavelength employed was 488 and 458 nm applied by a 40mW Argon laser (Argon Ion Laser System, Series IMA 100, Olympus). The 488 nm wavelength was used to visualise the endplate and both were used when bleaching a part of it.

2.7.1 Test of the stability of the micro spheres

The micro spheres used as controls were tested for bleaching by taking 5 times as many photos of one sphere as in a normal series (36x5=180), in rapid succession, Fig 2.2.

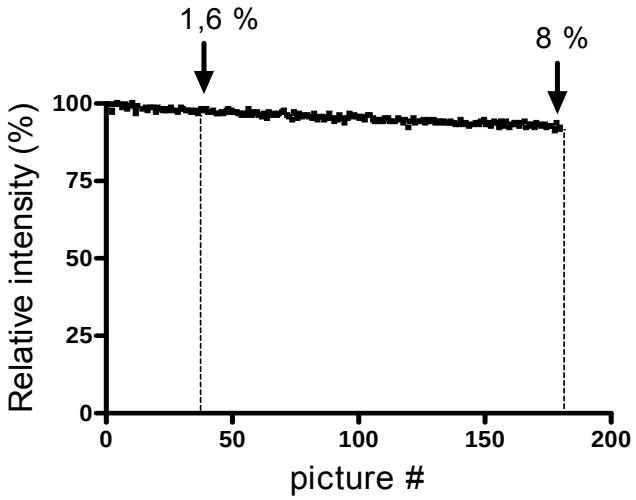

Figure 2.2 Bleaching test of micro spheres. In a normal picture series of an endplate 36 pictures were taken. Five times as many pictures, 180, were taken in rapid succession of a micro sphere. After 36 pictures there was a decrease in the relative intensity of 1.6% and after 180 pictures the decrease is 8%. The micro sphere was slightly bleached by the photographic process.

There was a decrease in the relative intensity of about 8% after 180 photos were taken. This means that a slight bleaching occurred during the photographing of the micro sphere. For the 36 photos taken in one experiment the average decrease was 1.6%. Thus the micro spheres can for practical purposes be regarded as photo-stable in these experiments, and were used as standards in these experiments.

2.7.2 Test of stability over time

To test the stability of the laser, microscope and recording system, a series of photos of a micro sphere was taken in the same way as in the experiment; three photos every 30 min for five hours. This was done on three separate days, Fig 2.3.

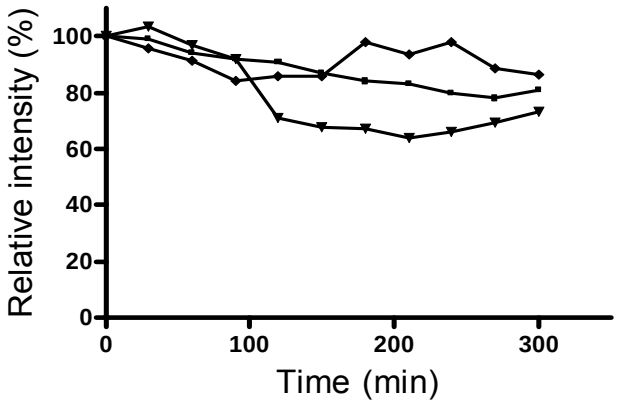

Figure 2.3 Stability of the microscope system over time. On three separate days pictures of a micro were taken sphere every 30 min. The change in the relative intensity of the constant fluorescent micro sphere varies between the three days.

The microscope system was not stable over time and the instability varied from day to day. There was a general decreasing tendency with an average total decreases of 20% and with fluctuations within this range. The photo was refocused each time to make sure the change was not due to drift in the focal plane and as demonstrated in Fig. 2.3, the decrease was not due to bleaching of the micro sphere, which can only account for 1.6% of the decrease.

Because of these problems the microscope was not considered suitable for these quantitative experiments at the time when the experiments were conducted. The microscope had just been acquired when these tests were conducted and later several new software editions have been installed. The system seems now to be more stable and will be used in later studies.

2.8 Quantitative fluorescence microscopy

When doing quantitative experiments it is important that there is as little variation as possible besides the actual parameter being measured. Therefore since the confocal microscope was not stable, a fluorescent microscope (Olympus BX50WI) with a SIT- (Silicon Intensified Tube) camera (Hamamatsu, C2400-08) was used to take the pictures for intensity analysis.

A 60x water immersion objective (Olympus, LUMPlan FI) was employed. A halogen lamp (Olympus, U-LH100) and filter cube XF22, BX096 (Omega Optical) was used to excite the EGFP with blue light and select the green light being emitted. The halogen lamp was connected to a voltmeter (Avo, Ltd. Dover, England 81217) to be certain that the same light

intensity was used to excite the EGFP throughout a series of an endplate. Variables of the microscope system were tested. All tests were conducted with the same filters and objective as used in the experiments.

2.8.1 Time-stable recordings with the SIT camera

The stability of the microscope, light source and the SIT camera was tested in the same way as described above, for the confocal microscope, (Fig. 2.4).

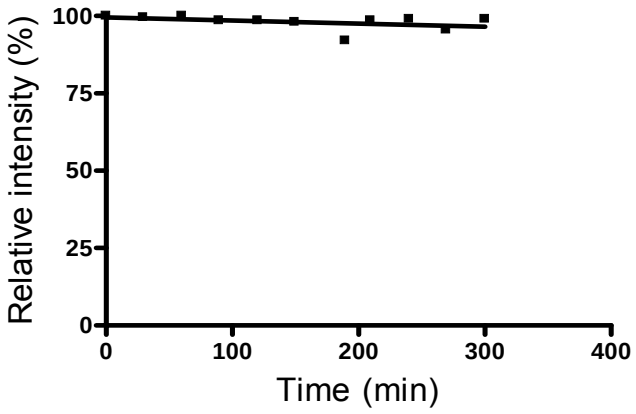

Figure 2.4 Stability over time with the SIT camera. A micro sphere was photographed every 30 min for 5 hours. The intensity for each time point is shown relative to the starting point intensity. There was a non-significant decrease in the relative intensity of the sphere.

There was a slight, non-significant decrease in the relative intensity over this time period. There are also slight variations with a maximum difference of 7%. To correct for this variability the micro spheres were used as a standard in the experiments for each photo taken.

2.8.2 Test of the stability of the micro spheres

Since the micro spheres do not get bleached when exited by the laser they are unlikely to be bleached by the much weaker halogen lamp, but this was still tested. When conducting a full experiment with this microscope the sphere is subjected to light for no more than 12 min. The test was conducted by taking three photos of the micro sphere in the z-plane. The light was left on for 15 min and three new photos taken and so on for 90 min, Fig 2.5. There was no

total decrease in intensity, but a slight non-significant increase. The spheres do not get bleached when exited by the halogen lamp.

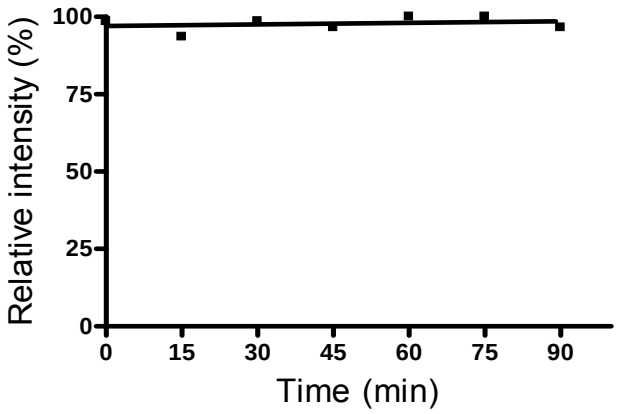

Figure 2.5 Test of micro spheres. Three pictures in the z-plane were taken of the micro sphere every 15 min and the light was left on between these pictures. Subjecting the micro spheres to the light used when taking pictures, for a total of 90 min did not bleach the spheres.

2.8.3 Linear response of the SIT camera to changes in light intensity

The response of the SIT camera was tested by placing different calibrated neutral filters in the light path. These let through 12, 25 and 50% of the light emitted. The test was done twice, with the two different offsets used in the experiments, 0.0 and 0.1.

The y-intercept of the graph corresponds to the actual offset of the system. Ideally this should be zero when the chosen offset is 0. The fact that the offset had a pixel value of 25 resulted in every measured value being 25 pixels over the actual value. This represents electrical noise. When measuring the pixel values of the experimental photos this was corrected for by subtracting the background value (section 2.9.3). Using two different offsets will not affect the results since the same offset is always used throughout an experimental series on one endplate.

For both of the chosen offsets (0.0 and 0.1) the relationship was linear (r^2 = 0.998 and 0.997 respectively). Fig. 2.6 show the linear relationship (for the offset of 0.0) between the light emitted and the light registered which is important for quantitative measurements. This ensures that slight variations in the intensity of the light-source over time, can easily be corrected for (explained in section 2.9.2).

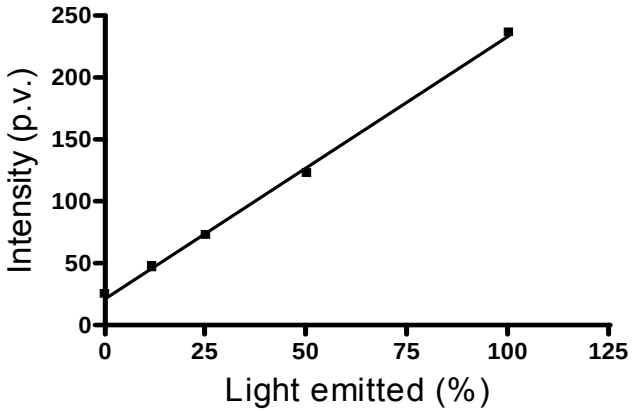

Figure 2.6 Linearity of the SIT camera. Pictures were taken of the light emitted from the trans halogen lamp when placing neutral filters calibrated for letting through 12, 25 and 50% of the emitted light. Pictures were also taken without any filter in the light path (100%) and with the light turned off (0%). Offset was set to 0.0 (or 0.1, not shown). The offset of the system has a pixel value of 25, the y-intercept of the graph.

2.8.4 Spatial uniformity measured in the SIT camera

The spatial sensitivity was tested by taking a photo of a white piece of plastic tape. Pixel values along a horizontal and a vertical line going through the centre of the picture plane were measured. The pixel values in the centre of the field were slightly higher than on the edges, still the part of the field used in the experiments showed very little variation (grey area in Fig. 2.7). The lamp and the camera have variations in this part of the field with a standard deviation of 4.9 pixel values on the 1-256 scale. To minimise the effect of these spatial variations in sensitivity between photos, the endplate or micro sphere was placed in the same position at every imaging time point.

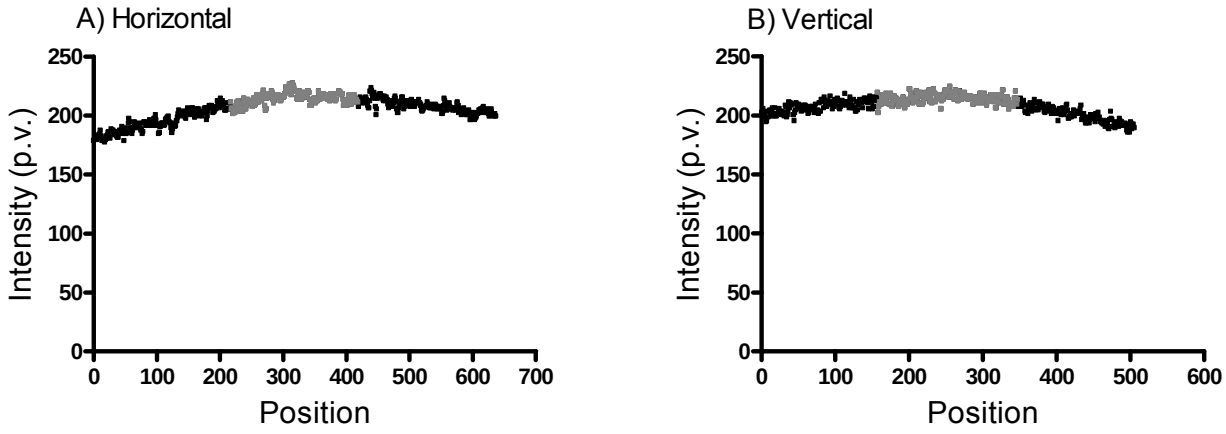

Figure 2.7 Spatial sensitivity. A picture was taken of a piece of white plastic tape. Horisontal A) and vertical B) lines were drawn to give intensity profiles. Grey area corresponds to the part of the picture plane used in the experiments.

2.8.5 Test of rapsyn-EGFP bleaching

To get correct results from the FRAP experiments it is also very important that the EGFP in the endplate is not being bleached when photographing. This would lead to a lower registered recovery than there actually was. This was tested in the same way as the micro spheres were tested, section 2.8.2. The endplate did not get bleached during photographing, Fig. 2.8. There was a slight increase in the relative intensity but no significant deviation from zero in the slope of the curve.

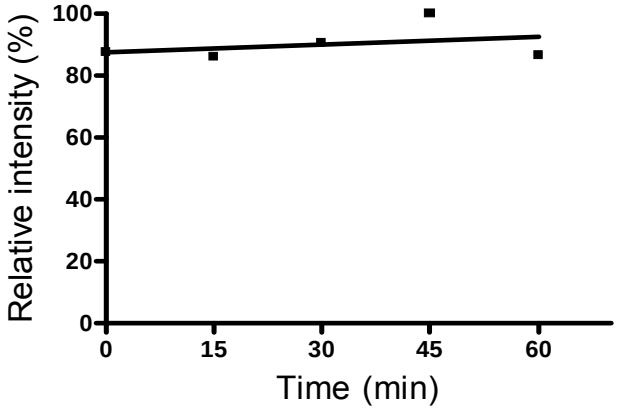

Figure 2.8 Test of bleaching on endplate with SIT camera. Photos were taken of the endplate every 15 min and the light was left on between each photos. Subjecting the endplate to the light used when taking photos, for a total of 60 min does not bleach the endplate.

Since the SIT camera is more stable than the confocal microscope this was used when taking the photos before and after photobleaching of the endplate. However the halogen lamp was not sufficiently strong to enough bleach the rapsyn-EGFP. This had therefore to be done with the laser on the confocal microscope. The mouse was transferred between microscopes before and after bleaching.

2.9 Data processing

2.9.1 Measuring micro spheres

As described in section 2.6.3 three photos in the z plane were taken at each time point. The photo from each series with the same focus planes was selected out of the three. Measurements were done in Fluoview (Olympus, FV 1000 software). The micro spheres were

measured by drawing a line through the centre of the sphere and obtaining an intensity profile with a width of 1 pixel from this, Fig. 2.9. The average of the line within the sphere was calculated.

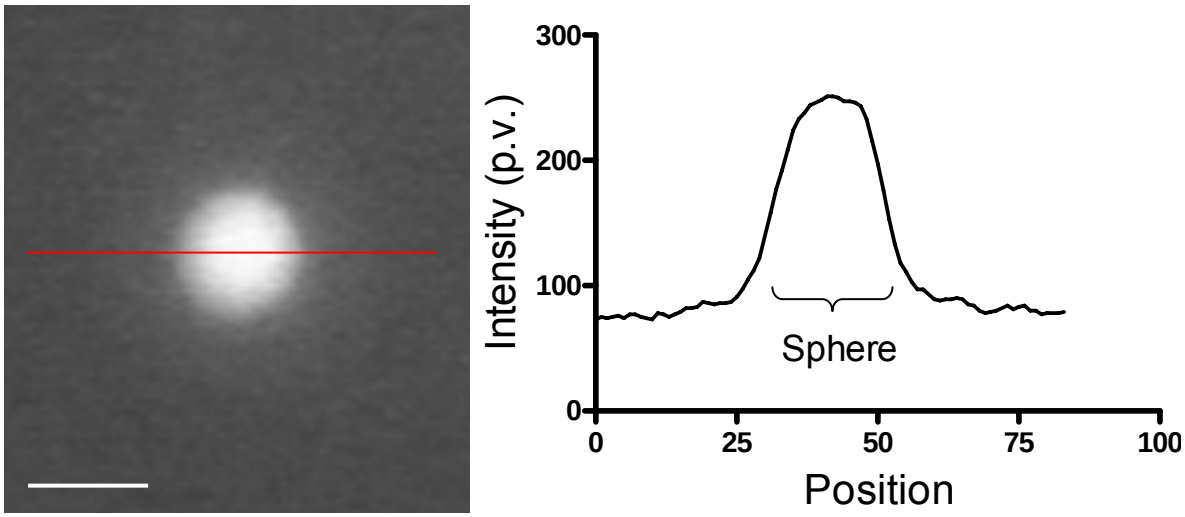

Figure 2.9. Micro sphere with associated intensity profile. For each micro sphere picture an intensity profile is obtained from a line (indicated in red) drawn through the centre of the sphere. Scale bar 5µm.

2.9.2 Endplate measurements

The different regions (bleached and unbleached) were ringed round and the size of the region obtained and found as a percentage of the total endplate area.

The intensity of the rapsyn- EGFP in a region of the endplate was found in the same way as with the micro spheres, a line was drawn over the area and the surrounding cytosol. An intensity profile was obtained and an average taken of the values in the desired ranges, Fig. 2.10.

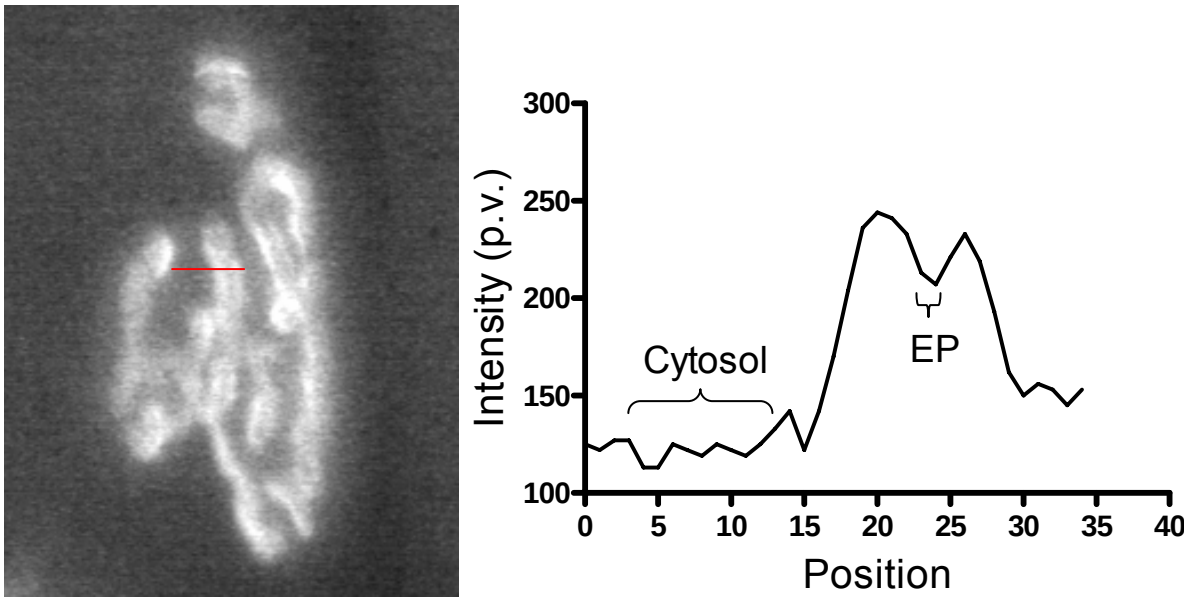

Figure 2.10 Endplate with associated intensity profile. Measurements of endplates were done by drawing a line (indicated in red) through the area to be measured (bleached or unbleached). The line gave the intensity profile on the left. Position 0-15 of the line was in the cytosol (non-cluster) portion in the picture, while 15-30 was in the endplate (EP) AChR cluster. The dip in the profile corresponds to the plateau in the endplate while the two peaks are where the folds in the endplate stoop, Fig. 1.1. The average cytosol value is subtracted from the average endplate value to give the actual endplate value as described in the next section. Scale bar 10µm.

2.9.3 Correcting for variations in the microscope system

The micro spheres were used to correct for variations in the microscope system. Any changes in the measured intensity of the spheres were due to changes in the microscope and must be corrected for. In some of the experiments the light emitted from the micro spheres was saturated and they could therefore not be used as controls. Instead cytosol was used as a control for these endplates. This was possible since, where the micro spheres varied, the cytosol always varied in the same way, as shown by the linear relationship between the pixel values of the spheres and of the cytosol, Fig. 2.11.

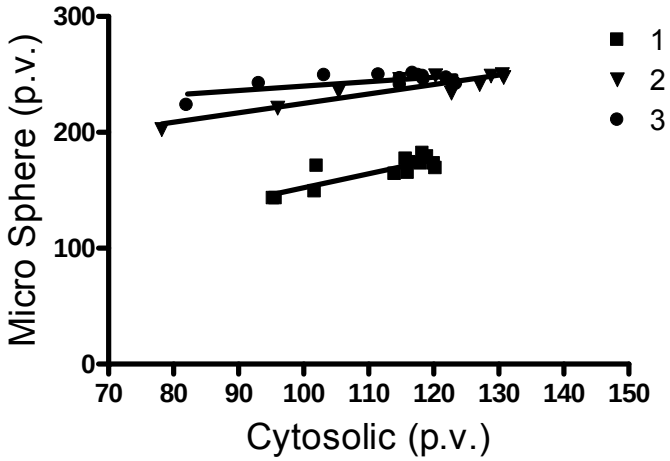

Figure 2.11 Relationship between micro sphere and cytosol. For each time point in three different experimental series the measured pixel value of the micro sphere was plotted against that of the cytosol. The square of correlation for experiments 1, 2 and 3 are 0.72, 0.85 and 0.44 respectively.

The pixel values for each endplate at time t were therefore corrected by multiplying by the fold-change in the control value (either micro sphere or cytosol) compared to the photo taken before bleaching. It was assumed that the cytosol was constant, since the measured intensity values for the cytosol followed the changes in the emitted light of the constant micro spheres.

$Ec_t = E_t*(K_p/K_t)$

E_t = endplate at time t
Ec_t = endplate corrected for control
K_p = control pre bleach
K_t = control at time t

The pre-bleach cytosol value (C_p) was used throughout a series since this is defined as constant. This constant cytosol value was then subtracted from the corrected endplate values for each time point to correct for background and offset of the microscope system.

$Ea_t = Ec_t - C_p$

Ea_t = actual endplate value at time t
C_p = pre-bleach cytosol value

2.9.4 Calculating recovery

The recovery at each time point was then calculated as follows. Ea_0, the actual endplate value just after bleaching (time 0), was subtracted from Ea_t, the endplate value at time t (corrected for variations and background). This was further divided by the Ea_p, the corrected pre-bleach endplate value. This was then converted into a percentage of the pre-bleach value.

$R_t = (Ea_t - Ea_0) / Ea_p$

$R_t\ (\%) = (R_t / R_p)*100\ \%$

R_t = recovery at time t
Ea_t = actual endplate value at time t
Ea_0 = Ea at time 0, after bleach
Ea_p = Ea pre bleach
R_p = recovery at pre bleach

This gives a pre-bleach value of 100 % and a time 0 value of 0 %.

2.9.5 Intensity in unbleached endplate areas

Endplate values were also measured in an area outside the one being bleached. This was done in the same way as described for the bleached areas above and also corrected in the same way for changes in the micro spheres or cytosol values. The intensity for each time point was then found as a percentage of the post-bleach measurement. Note that, for bleached areas, the intensity was found as a percentage of the pre-bleach value.

When bleaching an area, the boundary between the bleached area and the surroundings was also slightly bleached due to stray light. When the bleached area was large (with a correspondingly longer bleaching time) this boundary was larger. In cases where the muscle moved as well, due to the mouse's breathing movements, the boundary was even larger. The decrease in intensity in unbleached regions represents the biological processes under study that will be discussed in the next chapters. The initial drop in intensity in unbleached areas during the bleaching process however, was due to stray light bleaching during the bleaching process. Therefore the post-bleach intensity was set to 100%.

2.9.6 Graph associations

Graphs were plotted in GraphPad Prism 4. For the recovery-curves one- and two-phase exponential association graphs were plotted, either with no restrictions or Ymax forced to 100%. For the unbleached graphs a one-phase exponential decay fit was used. For each time point, the mean with the standard deviation bars are shown for all graphs.

2.9.7 Statistical analysis

An unpaired t-test was used to test the significance of the difference between the intensity decreases for endplates with a large or small area bleached. Paired t-tests were used to test the significance of the difference between time points within one group.

3 RESULTS

Twelve *edl* muscles were electroporated. This led to Rapsyn-EGFP expression in 10-40 fibres per muscle after 6-9 days. Only *en face* endplates were used for the FRAP experiments. All but one muscle displayed *en face* endplates on fibres expressing rapsyn-EGFP. On the other 11 muscles, 1-4 endplates were bleached, a total of 28 endplates. Of these, one was lost between bleaching and the taking of the first photomicrograph. Three of the fibres contracted spontaneously after the bleaching and subsequently segments of the fibres degenerated. Three fibres changed their position so that their endplates were no longer *en face*. Eleven endplates turned blurry during the course of taking the photo series. This blurriness could be caused by either technical or biological factors, presumably by damage to the fibres by the high light load. The three fibres that died all had large portions of their endplates bleached. These were subject to the laser for a prolonged period (section 2.6.1). It is likely that fibres with blurry endplates were also harmed by the high light intensity, but to a lesser extent. The remaining ten endplates constitute the data used in the analysis, Table 3.1.

Endplate no.	Bleached area (µm2)	Bleached potion of endplate area (%)	Small/large portion bleached	End time (min)	Pre-bleach pixel value	Post-bleach pixel value	End pixel value
1	71	6,8	Small	300	147	88	121
2	34	2,4	Small	300	92	82	86
3	35	2,8	Small	300	188	126	161
4	37	3,2	Small	270	194	107	139
5	59	5,4	Small	270	136	94	112
6	1000	96,8	Large	300	131	68	77
7	1232	88,1	Large	300	161	69	81
8	1530	82,8	Large	300	136	79	85
9	1236	70,3	Large	300	123	77	81
10	813	52,0	Large	300	112	74	79

Table 3.1 Experimental data. The ten endplates used in the analysis are listed with size of bleached areas, duration of imaging (end time) and pixel values for time points before and directly after bleaching as well as that corresponding to the "end time". The end time is the last time point recorded for the endplate. The pixel values were corrected for variations in intensity of the control as described in section 2.9.3, but without the background deduction. Pictures corresponding to time points of listed pixel values are shown in Fig. 3.1 and 3.2., for endplates with a small and large portion bleached respectively.

For each of the ten endplates pictures taken before (-10 min) and directly after the bleach (0 min) and at the last time point (270 or 300 min) are presented in the following figures. For all endplates except 4 and 5 the last time point was at 300 min (5 hours). Endplates 4 and 5 were in the same mouse, which died of an overdose of anaesthetic just before the 300 min time point. Endplates 1-5 had a small area bleached these are shown in Fig. 3.1 while endplate 6-10 with a large area bleached are presented in Fig. 3.2. The corresponding recovery curve for each endplate is also depicted with pixel values for each time point corrected for changes in the microscope system, as described in section 2.9.3, as described for Table 3.1.

The photomicrographs of the endplates presented in Fig. 3.1 and 3.2 were adjusted in Adobe Photoshop 7.0 according to the changes in pixel values of their corresponding cytosolic or micro sphere control. With the Brightness/Contrast command, the same brightness adjustment was made to every pixel in an image so that they corresponded to the pre-bleach picture which is unchanged for all endplates. The area which has been zoomed in on when the endplates were bleached is marked by a red square in all the photos (Fig. 3.1 and 3.2) the sizes of the squares are not absolutely proportional to the bleached area. As described in section 2.9.2 a line was drawn through the bleached area to give an intensity profile from which the pixel values were obtained.

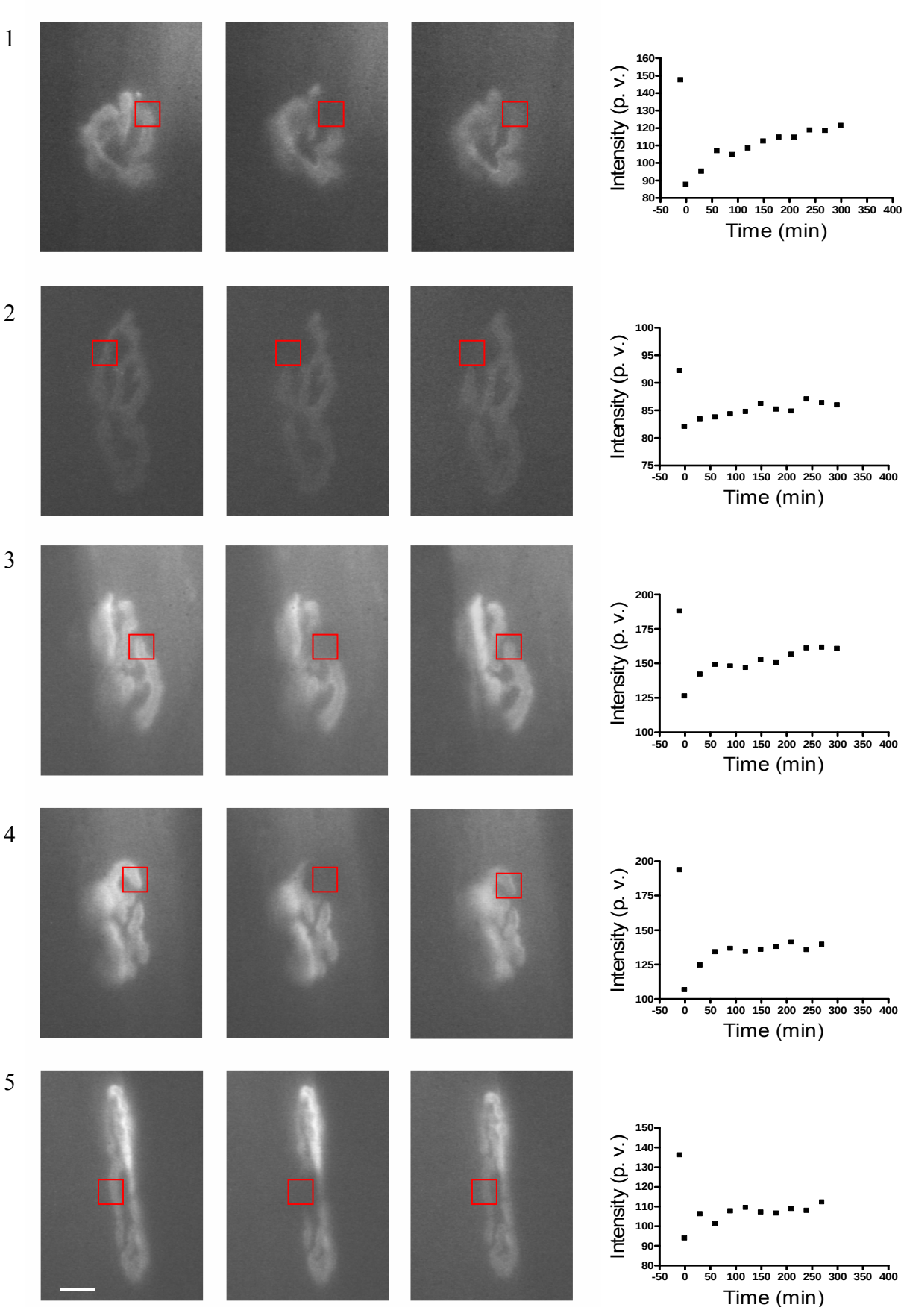

Figure 3.1 Endplates 1-5 with a small portion of the endplate bleached. Pre-, post-bleach and end photos from each series with corresponding recovery curves. Scale bar 10 µm for all photos. Endplates 1-3 have the last time point at 300 min, while endplates 4 and 5 go to 270 min. The photomicrographs were corrected for changes in intensity for its corresponding control and corrected pixel values (p.v.) were plotted in the graph, as explained in the text. Note that the scale of the Y-axis varies between graphs.

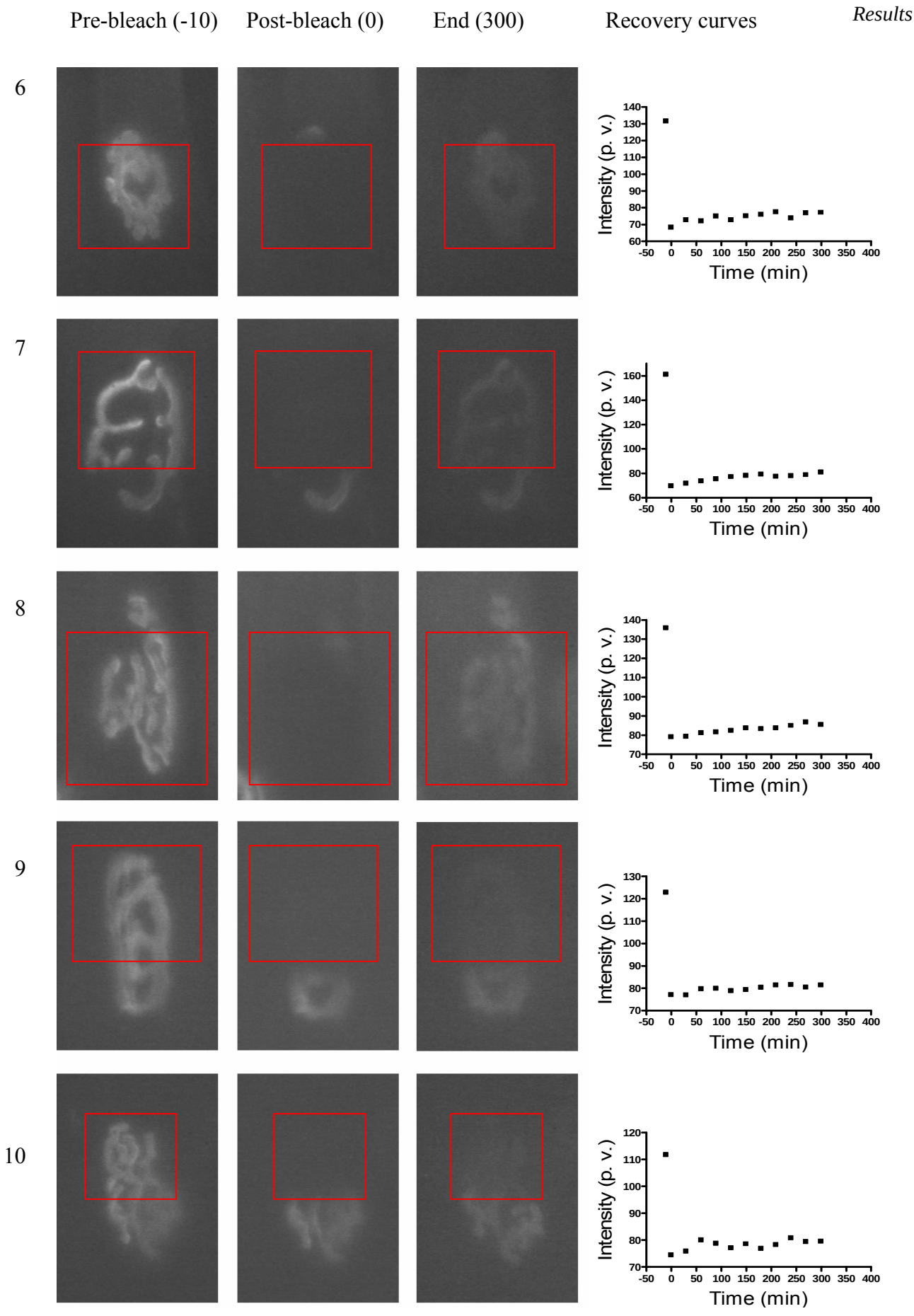

Figure 3.2 Endplates 6-10 with a large portion of the endplate bleached. Pre-, post-bleach and end pictures from each series with corresponding recovery curves. Scale bar 10 µm for all photos. All endplates go to 300 min. The photomicrographs were corrected for changes in intensity for its corresponding control and corrected pixel values (p.v.) was plotted in the graph, as explained in the text. Note that the scale of the Y-axis varies between graphs.

3.1 Changes in intensity of endplates 1-5 with a small portion bleached

3.1.1 Intensity changes of endplate no. 4

To better illustrate closer the changes in the intensity measured over the 5-hour period of the experiments, endplate no. 4 is presented as an example for endplates with a small portion bleached (Fig. 3.3 and 3.4). The bleached area of this endplate corresponds to 3.2% of the total endplate area. The photos were corrected for changes in their control (cytosol or micro sphere) as done for Fig. 3.1 and 3.2 and the contrast of all the photos was increased by the same amount to clarify the changes in intensity taking place through the series. Directly after the bleach (at 0 min) the bleached area (indicated with red square) was slightly darker than the surrounding fibre staining. Already after 30 min, a slight recovery was seen. This recovery strengthened increasingly up to the last photo taken at 270 min.

Changes in the measured intensities are shown below for bleached (Fig. 3.3A) and unbleached (Fig. 3.3B) areas. The end intensity for the bleached area was just under half way between the pre- and post-bleach intensities (Fig. 3.3A). This coincides with Fig. 3.4. The bleached region was not as strong in the final picture as it was before bleaching. The photos do not clearly illustrate the slight decrease in intensity of the unbleached region (area in which the line for the intensity profile was drawn as described in section 2.9.2 is marked with a blue square in Fig. 3.4 and Fig. 3.3B). As tested in section 2.8.5, this decrease did not represent bleaching of the endplate due to the photographic process.

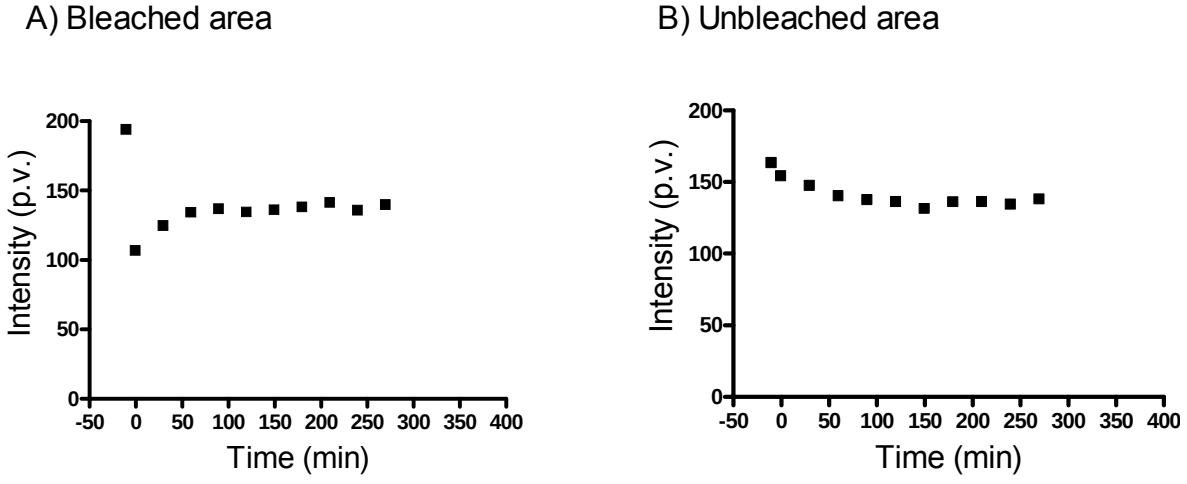

Figure 3.3 Changes in pixel values of bleached (A) and unbleached (B) areas of endplate no. 4. Graph A shows the changes in pixel values in the bleached area (red square in Fig. 3.4) from before the time of bleaching and up to the last time point at 270 min. Graph B shows the pixel values (p.v.) at the same time points, measured outside the bleached area (blue square in Fig. 3.4). The intensity of the bleached area just after the bleaching was 107 pixel values. This represents rapsyn-EGFP in the fibre as well as autofluorescence.

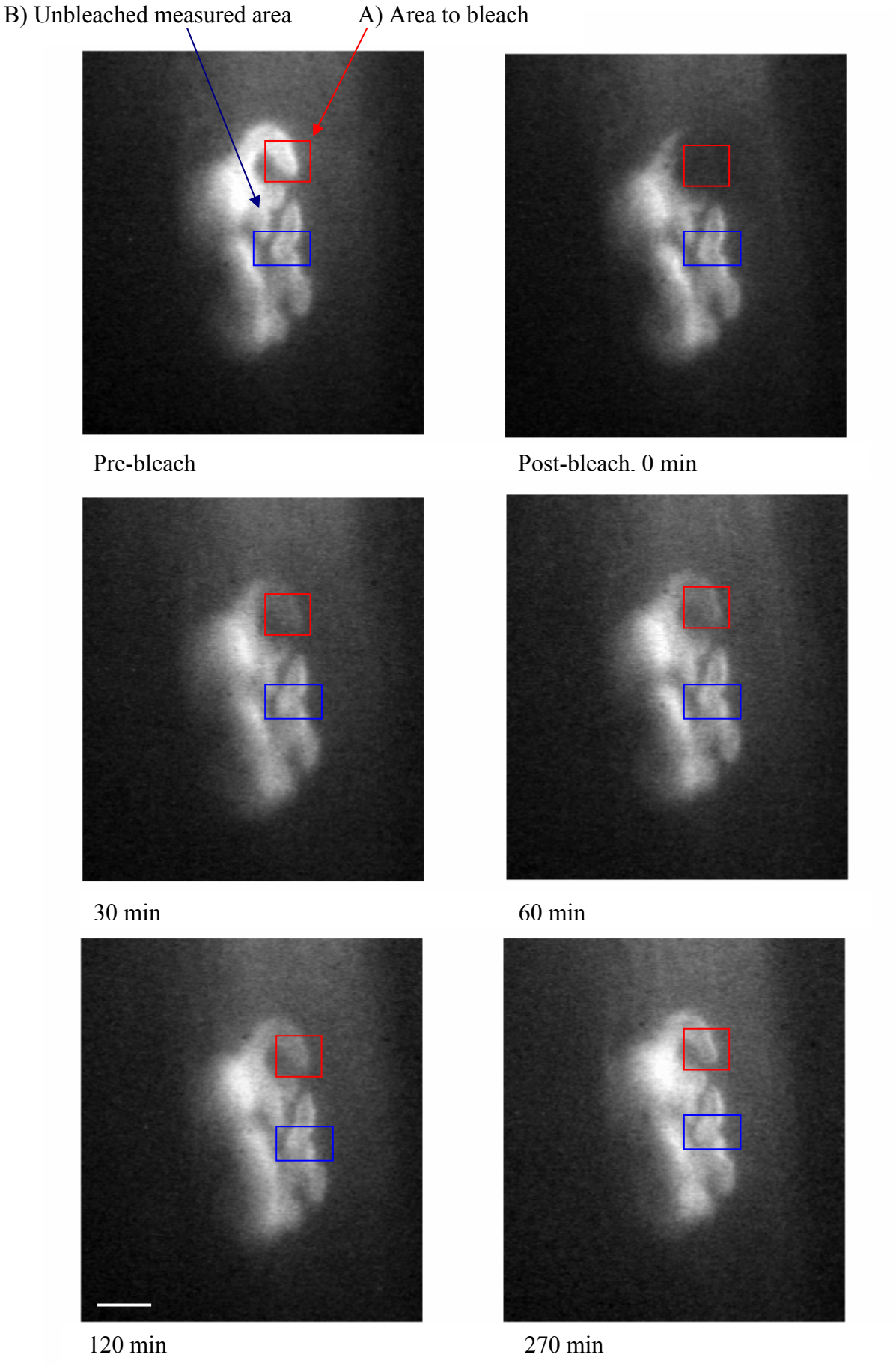

Figure 3.4 Time points in the series of endplate no. 4 where a small portion was bleached. The brightness was regulated according to the differences in the control measurements, as described in the text. The contrast was then regulated up with the same amount in all pictures. Areas A and B corresponds to graphs in Fig. 3.3 Scale bar 10 µm for all panels.

3.1.2 Recovery of small bleached endplate areas

To simplify comparisons between results of these and other experiments, the recovery was calculated as a percentage of the initial intensity, as described in section 2.9.4. One- and two-phase exponential fits for this relative recovery for endplates 1-5 are shown in Fig. 3.5. The two-phase exponential function did not converge with the data of endplates 2 and 5. A lack of convergence means that the program was not able to fit a two-phase exponential graph to these data.

For the one-phase exponentials the five endplates seem to split into two groups. Endplates 1-3 have Ymax1 ranging from 45-58% with a $t_{1/2}$ of 55-81 min (Table 3.2). Endplates 4 and 5 however have a lower Ymax of about 35%. This lower value is not due to the shorter time range of these experiments (Fig. 3.5).These endplates also have a markedly lower $t_{1/2}$ 1 of about 24 min, Table 3.2.

Endplate	**Exponential fit**	**Ymax 1± SEM (%)**	**Ymax 2± SEM (%)**	**$t_{1/2}$ 1 (min)**	**$t_{1/2}$ 2 (min.)**	**r^2**
1	**One-phase**	**57.54 ± 4.1**	-------	**79.59**	-------	**0.9619**
	Two-phase	85.78 ± 345.9	21.51 ± 37.3	410.3	25.97	0.9718
2	**One-phase**	**45.09 ± 7.0**	-------	**80.99**	-------	**0.8479**
	Two-phase	No convergence				
3	**One-phase**	**54.00 ± 4.6**	-------	**54.90**	-------	**0.8628**
	Two-phase	452.30 ± 9150	24.94 ± 9.7	2731	8.247	0.9537
4	**One-phase**	**35.93 ± 1.0**	-------	**23.31**	-------	**0.9659**
	Two-phase	17.48 ± 747.5	32.70 ± 18.7	680.4	19.79	0.9685
5	**One-phase**	**34.64 ± 2.8**	-------	**24.16**	-------	**0.7531**
	Two-phase	No convergence				

Table 3.2 Data of exponential fits for recovery of endplates 1-5. Maximal recovery (Ymax), half recovery time ($t_{1/2}$) and square of correlation (r^2) from graphs in Fig. 3.5 are shown. Ymax values are given with standard errors (SEM). All values for one phase exponentials are shown in bold text. For the two-phase exponential fits both of the two Ymax and $t_{1/2}$ values are given.

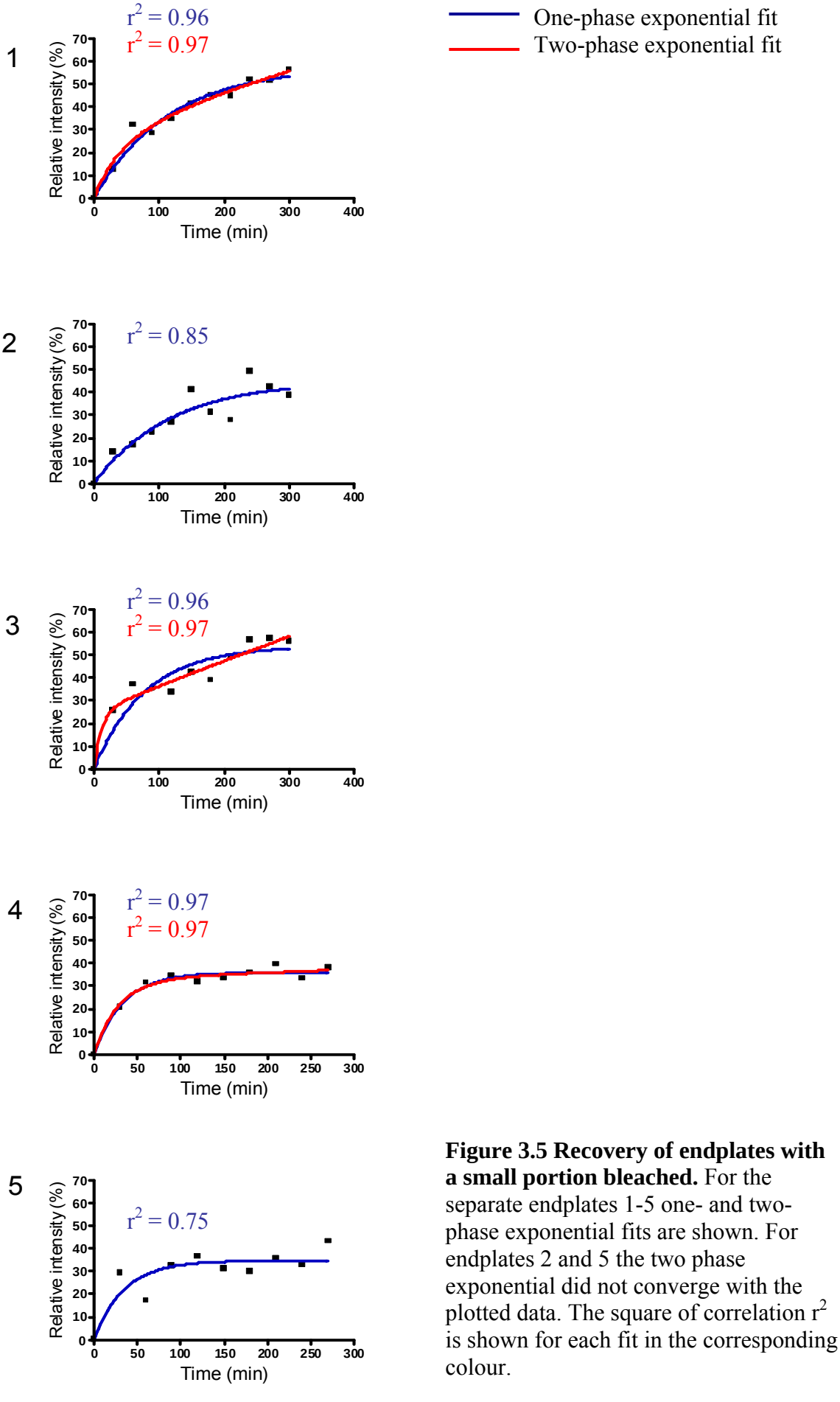

Figure 3.5 Recovery of endplates with a small portion bleached. For the separate endplates 1-5 one- and two-phase exponential fits are shown. For endplates 2 and 5 the two phase exponential did not converge with the plotted data. The square of correlation r^2 is shown for each fit in the corresponding colour.

Fig. 3.6 and Table 3.3 present pooled data of endplates 1-5. The data was plotted with a one-phase (Fig. 3.6A + B) and a two-phase (Fig. 3.6C) exponential fit. For graphs A and C the best fit for the graph is shown. For graph B however Ymax is set to 100% to see if the recovery was likely to have been total.

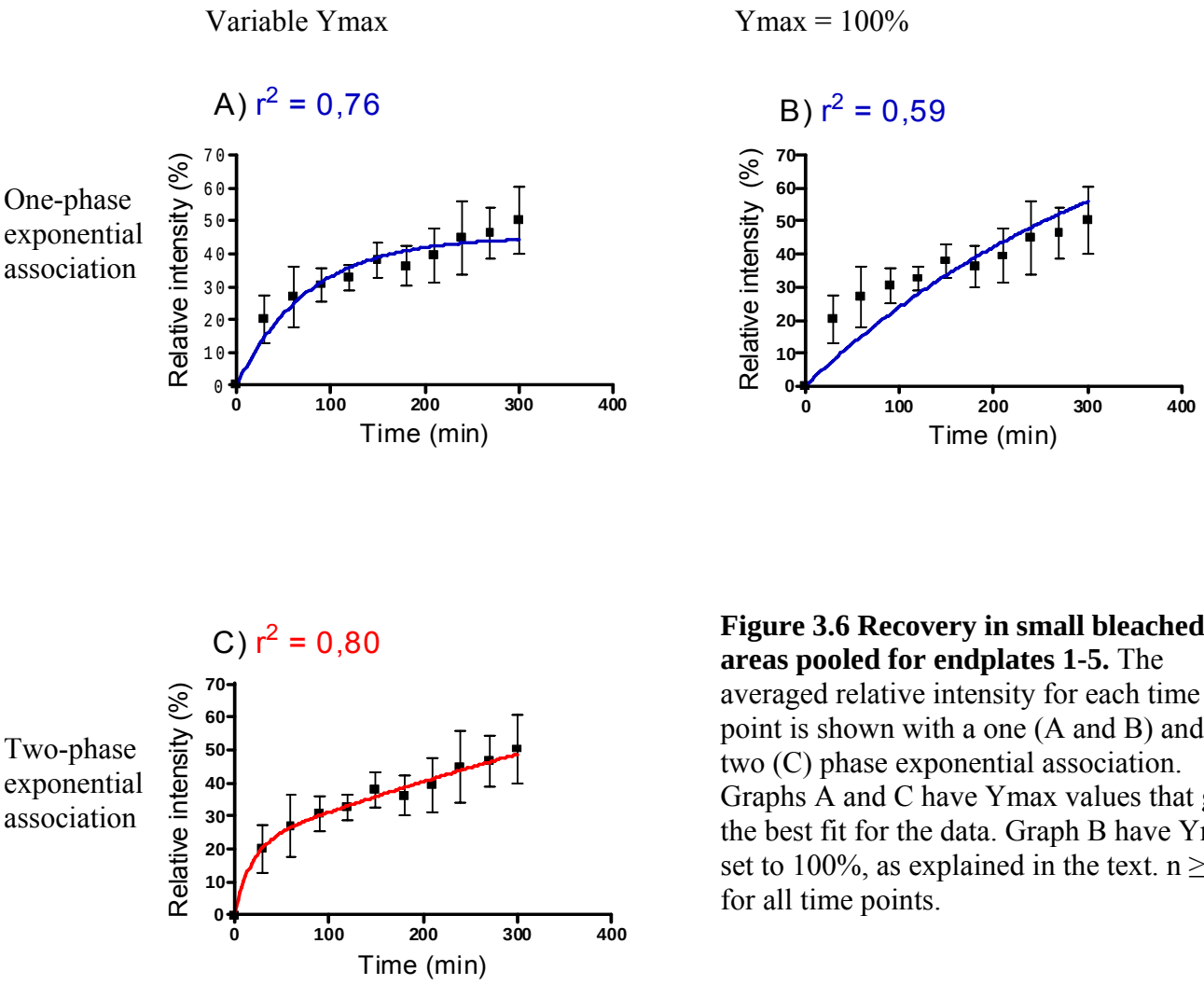

Figure 3.6 Recovery in small bleached areas pooled for endplates 1-5. The averaged relative intensity for each time point is shown with a one (A and B) and a two (C) phase exponential association. Graphs A and C have Ymax values that gave the best fit for the data. Graph B have Ymax set to 100%, as explained in the text. $n \geq 3$ for all time points.

Graph	**Exponential fit**	**Ymax 1 ± SEM (%)**	**Ymax 2 ± SEM (%)**	**$t_{1/2}$ 1 (min)**	**$t_{1/2}$ 2 (min)**	**r^2**
A	One-phase	45.16 ± 2.4	___	52.87	___	0.7634
B	One-phase	100	___	253.6	___	0.5941
C	Two-phase	108.4 ± 511.3	20.98 ± 9.753	702.2	11.98	0.8036

Table 3.3 Data of exponential fits pooled from endplates 1-5. Maximal recovery obtained with the graph fit (Ymax), the half recovery time ($t_{1/2}$**)** and the square of correlation (r^2) values are listed for the graphs in Fig. 3.6. Standard error of mean (SEM) is shown for Ymax values. For graph B Ymax was set to 100% and therefore has no standard error.

The subjective impression was that the fit of the two-phase exponential (Fig. 3.6C) was better than the one-phase exponential (Fig. 3.6A). The square of correlation (r^2) however was only slightly different. The difference in square of correlation was much larger between variable and restricted Ymax for the one-phase exponential graphs (Fig. 3.6A and B).

The good two-phase exponential fit seen for the pooled data of endplates 1-5 (Fig. 3.6) was not reinforced when looking at the individual endplates (Fig. 3.5). The two phases in Fig. 3.6C was a result of the variations in half recovery time between the different data pooled in the graph as mentioned in the beginning of this section. Endplates 1-3 had a large recovery with a correspondingly long half recovery time (~54-80 min), while endplates 4 and 5 reached a lower Ymax with a much shorter half recovery time (~24 min). These differences explained the "poor" fit of the one-phase exponential to the polled data.

3.2 Changes in intensity of endplates 6-10 with a large portion bleached

3.2.1 Intensity changes of endplate no 7

Photos of endplate no. 7 are presented in Fig. 3.7, as an example of the endplates which have a large portion bleached. The bleached area of this endplate constituted 88% of the total area (red square in Fig. 3.7). There was a barely visible recovery after 30 min (not shown), and slightly more visible at 60 min. The recovery then increased slightly through the series up to the last photo at 300 min. It appeared as if the recovery was quicker in the outer regions of the endplate structure than in the centre (Fig. 3.7).

Comparing the last picture with the first (Fig. 3.7), showed that the recovery was far from complete, not even close to half of the initial intensity as is confirmed when looking at the slight increase in Fig. 3.8A. The intensity in the unbleached area decreased slightly (Fig. 3.8B and blue square in Fig. 3.7).

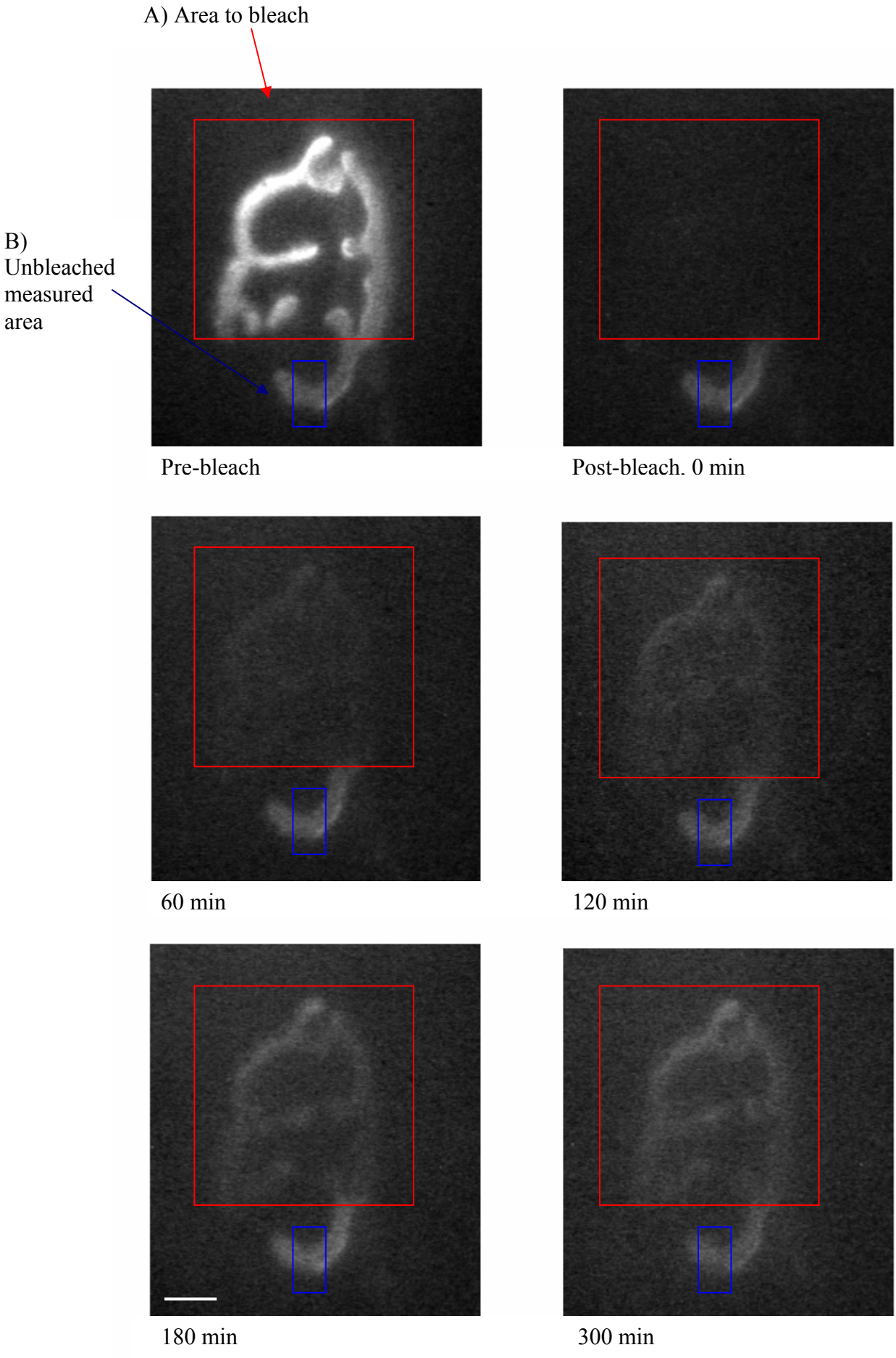

Figure 3.7 Time points in the series of endplate no. 7 where a large portion was bleached. The brightness was regulated according to the differences in the control measurements, as described earlier. The contrast was then regulated up with the same amount in all photos. Areas A and B corresponds to graphs in Fig. 3.8. Scale bar 10 µm for all panels.

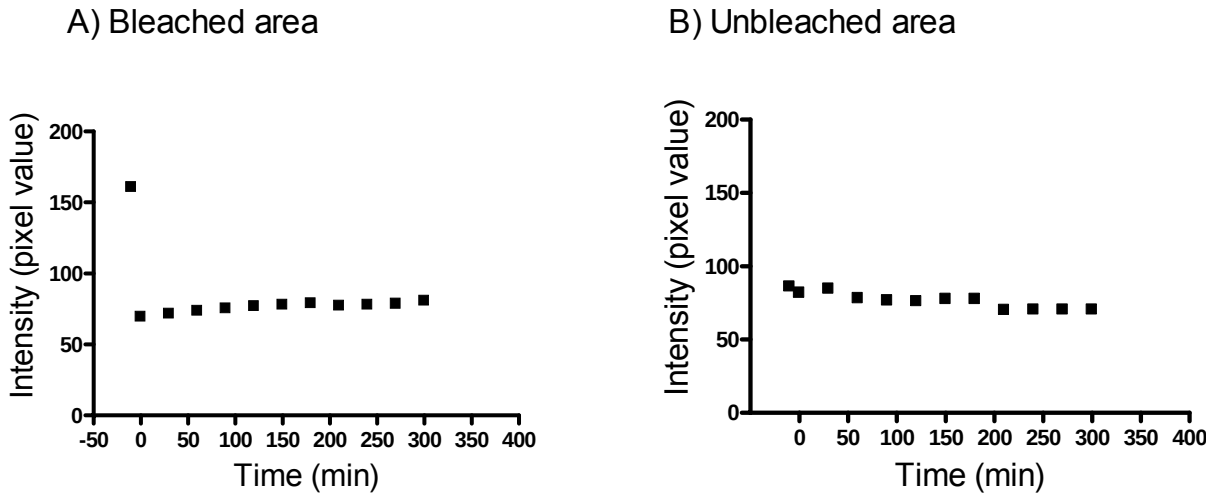

Figure 3.8 Changes in pixel values of bleached (A) and unbleached (B) areas of endplate no. 7. Graph A shows the changes in pixel values in the bleached area (red square in figure 3.7) from before bleaching and up to the last time point at 300 min. Graph B shows pixel values at the same time points measured outside the bleached area (blue square in Fig. 3.7).

3.2.2 Recovery of large bleached endplate areas

Separate graphs for the recovery of endplates 6-10 were plotted with one- and two-phase exponential fits (Fig. 3.9). The two-phase exponential association did not converge with the data of endplate 6. Table 3.4 lists maximal recovery (Ymax), half recovery time ($t_{1/2}$) and square of correlation (r^2) for the graphs in Fig. 3.9. Except for endplate 8, Ymax lies at about 12% for all of the endplates which have a large portion bleached. The half recovery times however vary a lot more, 25-107 min, for these endplates. Endplate 8 has a higher recovery with Ymax = 30%.

Endplate	Exponential fit	Ymax 1± SEM (%)	Ymax 2± SEM (%)	$t_{1/2}$ 1 (min)	$t_{1/2}$ 2 (min)	r^2
6	**One-phase**	**12,98 ± 1.5**	-------	**52,24**	-------	**0,7641**
	Two-phase	No convergence				
7	**One-phase**	**11,76 ± 1.0**	-------	**78,92**	-------	**0,9431**
	Two-phase	39,98 + 30507	9,109 ± 86.7	3567	62,53	0,9438
8	**One-phase**	**30,30 ± 21.9**	-------	**395,5**	-------	**0,9410**
	Two-phase	21,87 + 21993	31671 ± 5e+11	328,1	3,098e+006	0,9410
9	**One-phase**	**10,90 ± 2.9**	-------	**107,2**	-------	**0,8063**
	Two-phase	11,02 + 14.7	2,315 ± 67.0	198,6	36,92	0,8073
10	**One-phase**	**11,94 ± 1.5**	-------	**24,70**	-------	**0,5488**
	Two-phase	69,63 ± 12338	8,560 ± 14.7	2818	14,89	0,5902

Table 3.4 Data of exponential fits for recovery of endplates 6-10. Maximal recovery (Ymax), half recovery time ($t_{1/2}$) and square of correlation (r^2) from graphs in Fig. 3.10 are shown. Ymax values are given with standard errors (SEM).Values for one-phase exponentials are shown in bold text. For the two-phase exponential fits, both of the two Ymax and $t_{1/2}$ values are given.

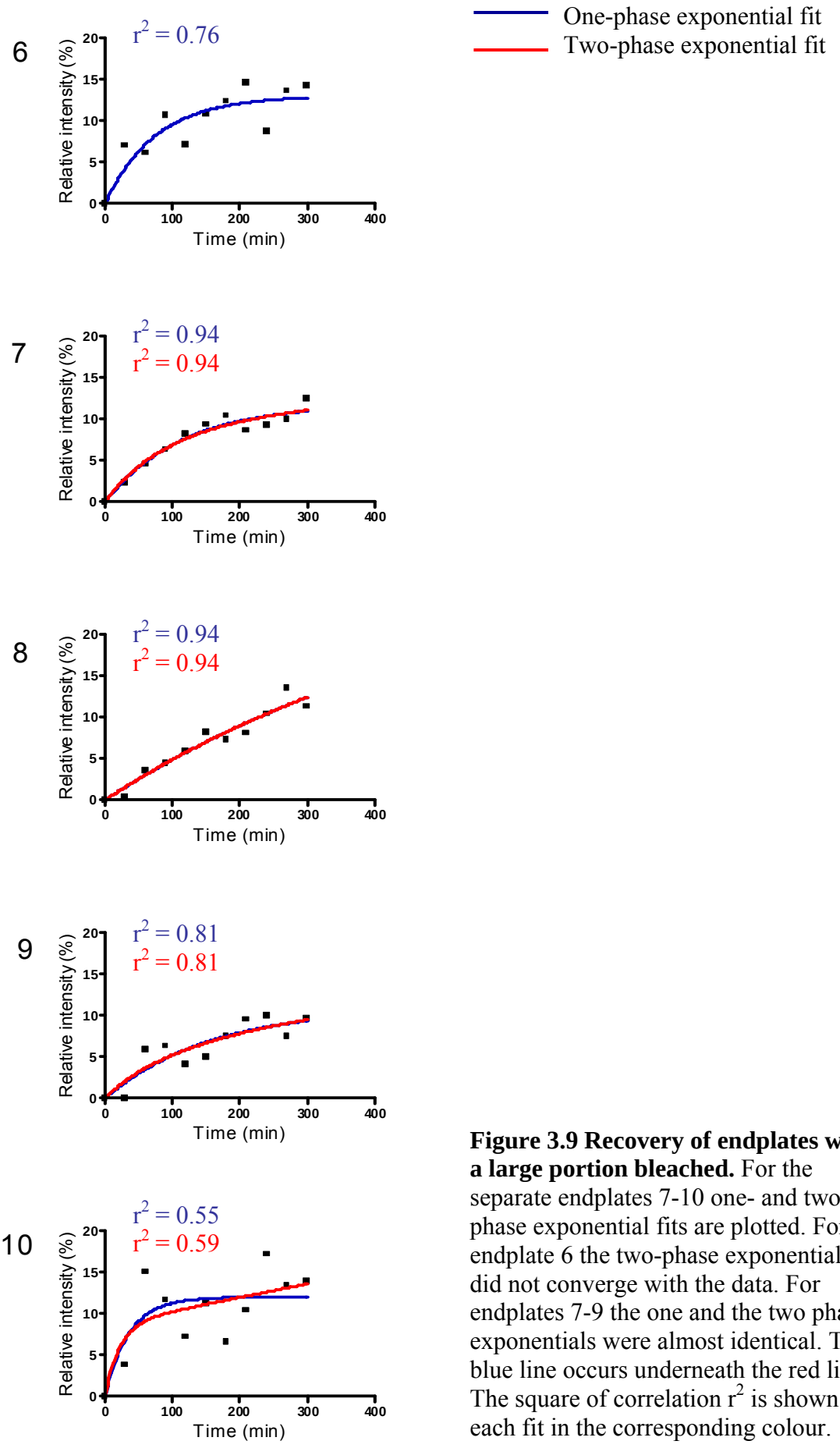

Figure 3.9 Recovery of endplates with a large portion bleached. For the separate endplates 7-10 one- and two-phase exponential fits are plotted. For endplate 6 the two-phase exponential fit did not converge with the data. For endplates 7-9 the one and the two phase exponentials were almost identical. The blue line occurs underneath the red line. The square of correlation r^2 is shown for each fit in the corresponding colour.

The pooled data of the endplates 6-10 was plotted with one-phase (Fig. 3.10 A and B) and two-phase (Fig. 3.10 C) exponential fits, as done for endplates 1-5 in Fig. 3.6. For graphs A and C, the Ymax gave the best fit for the graph, while for graph B,m Ymax was forced to go to 100%. The square of correlation was almost equal for the one- and two-phase exponential fit (~0.65, Fig. 3.10A and C) while, when setting Ymax = 100%, the square of correlation was only 0.51 (Fig. 3.10B). These and other data of the graphs are listed in Table 3.5.

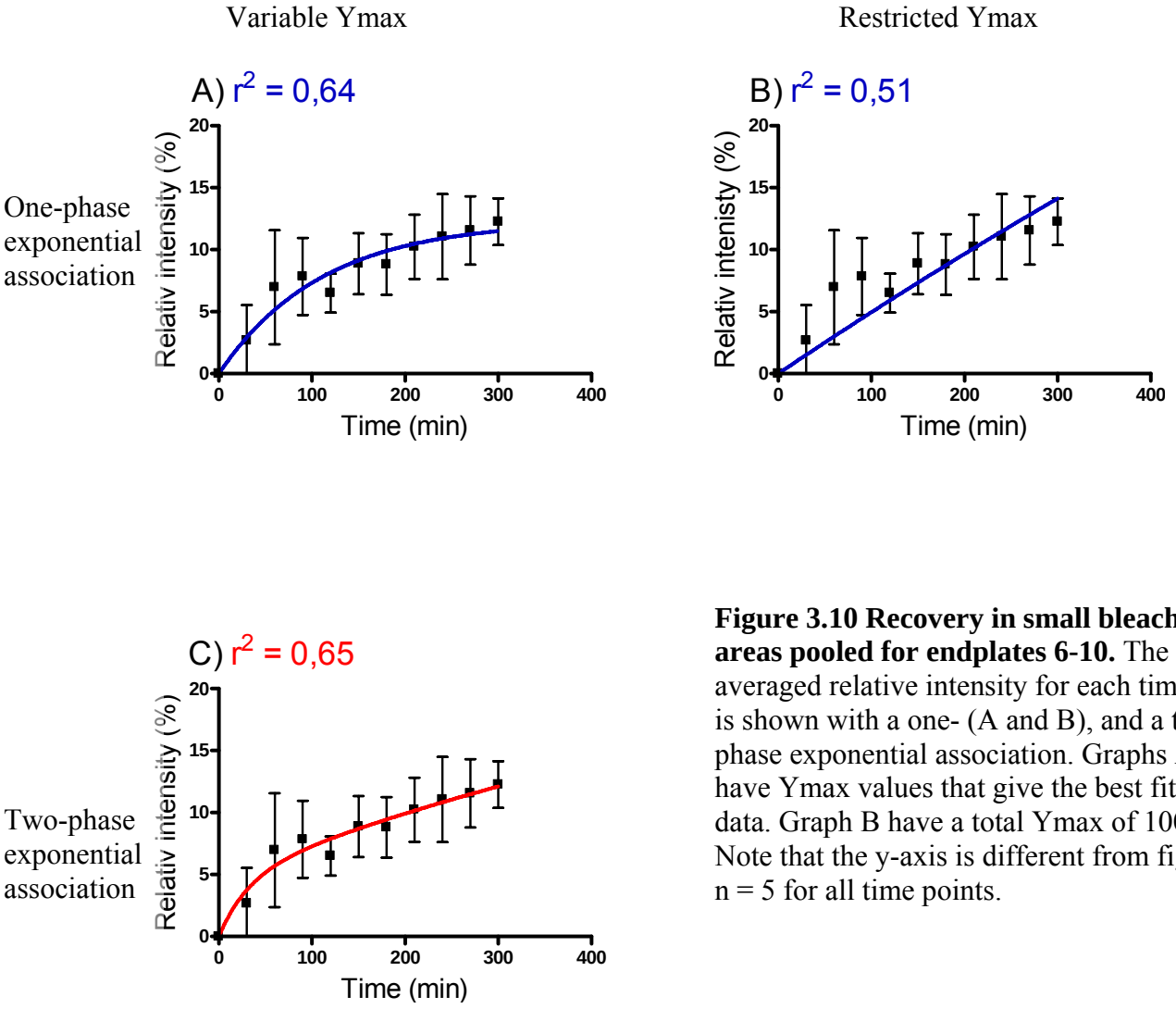

Figure 3.10 Recovery in small bleached areas pooled for endplates 6-10. The averaged relative intensity for each time point is shown with a one- (A and B), and a two- (C) phase exponential association. Graphs A and C have Ymax values that give the best fit for the data. Graph B have a total Ymax of 100%. Note that the y-axis is different from figure 3.6. n = 5 for all time points.

Graph	Exponential fit	Ymax1 ± SEM (%)	Ymax2 ± SEM (%)	$t_{1/2}$ 1 (min)	$t_{1/2}$ 2 (min)	r^2
A	One-phase	12.32 ± 1.294	___	76.71	___	0.6375
B	One-phase	100	___	1364	___	0.5059
C	Two-phase	24.80 ± 200.0	4.702 ±8.468	585.9	21.90	0.6522

Table 3.5 Data of exponential fits pooled for endplates 6-10. Maximal recovery obtained with this graph fit (Ymax), the half recovery time ($t_{1/2}$**)** and the square of correlation (r^2) values are shown for the graphs in Fig. 3.10. Standard error of mean (SEM) is shown for Ymax values. For graph B Ymax was set to 100% and therefore has no standard error.

Even though there were large differences in half recovery time between the one-phase exponentials for individual endplates (Table 3.4), the two-phase exponential fit was no better than the one-phase exponential fit for the pooled data (Fig. 3.10). It was therefore assumed that this was a single exponential process, as done with endplates 1-5.

Within both groups of endplates there appeared to be large variations in half recovery time between the endplates, even though Ymax only varied slightly between endplates 6-10. These differences might indicate actual biological divergence between the endplates though this did not seem to correspond with variations in amount of rapsyn-EGFP in the endplate (Fig 3.1 and 3.2).

3.3 Decrease in intensity of unbleached endplate areas

The changes in the intensity of unbleached areas during the 5 hours following bleaching was measured and calculated as described in section 2.9.5. A decrease in intensity was observed in all endplates. Fig. 3.11 shows this decrease for pooled data of endplates 1-5 and 6-10 as a percentage of their post-bleach intensity.

There was a decrease in relative intensity from the pre- (-10 min) to post-bleach (0 min) time point of 5.7% and 25% for endplates 1-5 and 6-10 respectively (Fig 3.11A and B). This decrease was due to slight bleaching in "unbleached" areas during the bleaching process because of stray light and movement of the muscle as described in section 2.9.5. For endplates 1-5 the decrease is small because of the unbleached measured area is distant from the bleached area and therefore is only influenced slightly by stray light. Endplates 6-10 however, had unbleached areas close to the bleached area and these ended up directly underneath the laser upon large movements of the *edl*, caused by the mouse breathing. This movement varied between animals. Endplate 8 was excluded from the analysis because, as shown in Fig. 3.2, the unbleached area of this endplate was almost entirely bleached as a result of the extensive movement of the muscle due to breathing.

One-phase exponential decays were plotted without considering this initial decrease. For endplates 1-5 it declined to a plateau at 67.7± 3.8% of the post-bleach intensity with half time of 49.3 min (Fig. 3.11A and Table 3.6) while for endplates 6-10 it declined to a plateau at 45.6 ±5.8 % with half time of 68.3 min (Fig. 3.11B). A two-phase exponential decay did not converge with the data.

A t-test was used to compare the intensity at time 0, after the bleach, with the final time point (the 270 min time point was used for endplates 1-5). There was a significant decrease for both of the endplate groups ($p = 0.019$ and 0.0004 for endplates 1-5 and 6-10 respectively). The difference in decrease between the two groups was also significant ($p = 0.02$). As explained for endplate no. 4, section 3.1.1, the decrease was not caused by bleaching of the endplate as a result of the photographic process. No decrease was evident even after exposure to the light for several times longer than the time used for a normal series (section 2.8.5).

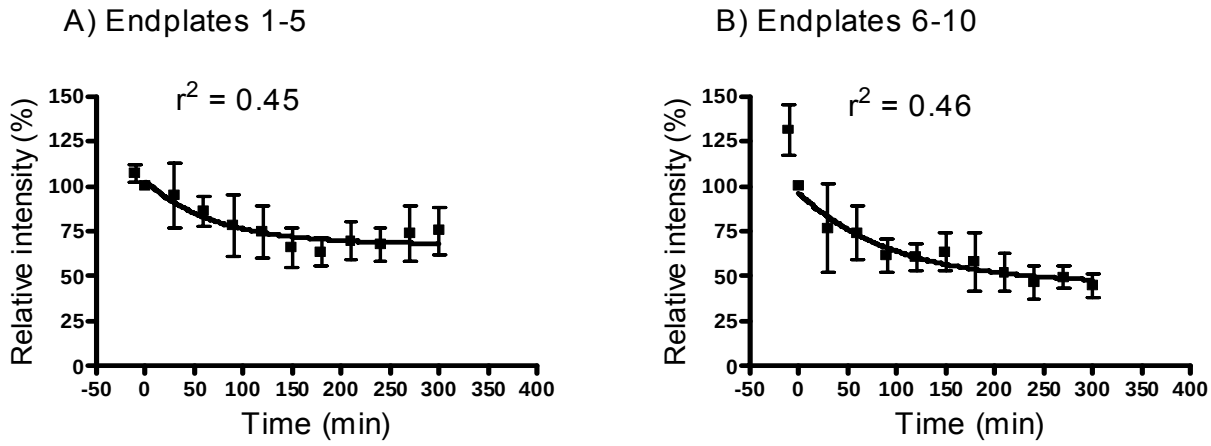

Figure 3.11 Decrease in relative intensity of unbleached areas of all endplates. Changes in intensity measured outside the bleached areas of endplates 1-5 (A) and 6-10 (B) are pooled and a one phase exponential decay plotted. As explained in the text, endplate 8 is excluded from the pooling of data from endplates 6-10. $n \geq 3$ for all time points.

Endplate	Plateau ± SEM (%)	$t_{1/2}$ (min)	r^2
1	60.77 ± 6.371	43.52	0.5983
2	81.85 ± 14.37	65.19	0.3153
3	67.85 ± 3.792	44.50	0.7611
4	64.08 ± 2.188	32.59	0.9138
5	60.11 ± 9.128	71.60	0.8260
6	52.78 ± 5.582	44.74	0.7389
7	-73.57 ± 358.5	439.2	0.8210
8	113 ± 1.386e+9	6.931e+6	-3.4e-5
9	53.86 ± 5.020	38.07	0.6843
10	47.18 ± 2.635	18.93	0.8660

Table 3.6 Data for one phase exponential decay of unbleached areas of all endplates. When plotting one phase exponential decays for unbleached areas of endplates 1-10 all endplates (except no. 8) show a decrease in relative intensity of unbleached areas (18-53%), graphs not shown. Endplate 8 (shown in grey) is excluded when pooling the data as described in the text.

The decrease in the unbleached areas was not proportional to the size of the bleached or unbleached areas. If the bleached and unbleached molecules are all distributed evenly throughout the endplate, the plateau of the decay curves should correspond to the portion of the unbleached areas. On average 4% and 78% of endplates 1-5 and 6-10 respectively were bleached. This leaves 96% and 22% of the total endplate that are not bleached for the two groups. These figures correspond to the minimum plateau caused by random exchange of bleached and unbleached molecules. However, the plateaux of 67.7% and 45.6% reached for endplates 1-5 and 6-10 respectively was lower for the first group (96%) and higher for the second group (22%) indicating a large contribution of some FRAP independent factor.

Possibly, a small portion of the decrease was due to unbleached rapsyn-EGFPs migrating into the bleached area in exchange for bleached molecules and in this way contributing to the recovery of the bleached areas. The major portion however, can be attributed to the FRAP independent process. This is supported by the findings that, when an endplate was followed for five hours as in the FRAP experiments but without bleaching any part of it, there was a similar decrease in intensity of the whole endplate down to ~40% (data not shown). This was also the case when taking a photo of an endplate, leaving it for five hours and taking another photo.

When tagging the receptors of the endplate with alexa-594-α-BuT, a similar decrease was detected both when pictures were taken every half hour and when a picture was taken only before and after the five hours. The decrease in intensity of rapsyn-EGFP and alexa-594-α-

BuT marked AChR was the same within the same endplate, but varied between endplates (Kristin Jensen, private communication).

Further, the same results were found when using the confocal microscope as when using the fluorescent microscope with the SIT camera, which indicates that the decrease cannot be related to the microscope system. This, and the fact that there was a decrease seen in unbleached rapsyn-EGFP and for α-BuT marked receptors, indicates that the decrease was unrelated to the FRAP experiments and bleaching caused by the photographic process, since no decrease is seen when subjecting the endplate to the same amount of light over a shorter time period (section 2.8.5). Why did we find this substantial decrease? It seems as if the change is highly related to the time range of the experiments.

In addition to rapsyn, agrin and the rest of the molecules at the endplate, activity in the muscle is crucial for obtaining and sustaining the high density of receptors found at the neuromuscular junction (Akaaboune *et al.*, 1999). When the AChR are blocked with α-BuT their half-life in the endplate is severely reduced and there is a reduction in AChR labelling of 0.13-4% per hour depending on the time since the blockade. However upon electrically stimulating the muscle, while the receptors are blocked, no such decrease is evident (Akaaboune *et al.*, 1999).

When we conducted FRAP experiments on rapsyn the mouse was anesthetised during the whole five hours of recordings. This means that there was no activity in the motor neuron innervating the muscle being observed. One would assume that this would leed to a decrease in receptor labelling and maybe also account for the reduction in rapsyn-EGFP staining. However, the decrease in the relative intensity of about 5% per day seen when applying a non-blocking dose of α-BuT, is not accelerated when also blocking totally with tetrodotoxin (TTX) (Akaaboune *et al.*, 1999). Anesthetising the animal is therefore not likely to cause a reduction in the relative intensity of rapsyn-EGFP or α-BuT marked receptors of more than 1% during the five hours we used to conduct the experiments, since TTX blockade inhibits nerve activity by blocking voltage gated Na+ channels (Akaaboune *et al.*, 1999). This cannot explain the large decrease seen.

Is it possible that the decrease seen is due to damage to the muscle fibres, independent of the amount of light received, for instance by the ringer lactate or low blood flow? To find the answer to these questions several further studies need to be conducted. The decrease seen in the unbleached areas of bleached and unbleached endplates, are also likely to occur in bleached regions and thereby disguise some of the recovery in these areas. Assuming that the same rate of loss occurred within the bleached areas, the actual recovery might have been 20-50% higher than that indicated in the beginning of the results chapter.

3.4 Total endplate recovery

By adding the percentage of the decrease at every time point for each endplate, a larger recovery was obtained (Fig. 3.12, graphs of individual endplates not shown). Endplates 1-5, which had a small portion bleached, reached an average Ymax of 79%, while for endplates 6-10, which had a large portion bleached, the average Ymax was 57% (Table 3.7). The difference, between the two groups in recovery at 270 min, is no longer significant ($p = 0.3$).

Endplate	End time (min)	End recovery (%)	Ymax ± SEM (%)	$t_{1/2}$ (min)	r^2
1	300	94.4	94.34 ± 7.320	58.88	0.9106
2	300	50.4	65.63 ± 26.36	94.57	0.6342
3	300	79.5	85.21 ± 3.920	48.73	0.9493
4	270	68.1	72.01 ± 1.624	28.95	0.9819
5	270	68.9	75.27 ± 3.837	54.24	0.9668
Average of 1-5	**270**	**72.7**	**78.49 ± 8.612**	**57.07**	**0.8886**
6	300	62.3	59.64 ± 4.925	43.24	0.8234
7	300	69.8	255.3 ± 490.4	609.8	0.8649
8	300	-173.7	-171.8 ± 13.24	32.53	0.8026
9	300	63.0	47.60 ± 22.82	55.02	0.4950
10	300	77.4	64.80 ± 3.065	20.09	0.8700
Average of 6-10	**300**	**68.1**	**57.35 ± 10.27**	**39.45**	**0.7295**

Table 3.7 Data for total recovery of individual endplate. When plotting one-phase exponential associations to the recovery corrected for the decrease in intensity of the endplate, the recovery ranges from about 50-100% (graphs not shown). End recovery, corresponding to the end time point (as in Table 3.1) is shown for all endplates. The average end intensity is found at the 270 min time point for endplates 1-5 and at 300 min for endplates 6-10. Endplate 7 (shown in grey) is excluded from the average Ymax, half recovery time ($t_{1/2}$**)** and the square of correlation (r^2), since the Ymax is so much higher than the rest, but not from the average end recovery. Endplate 8 (shown in grey) is excluded from all averages and when pooling the data, as described previously in the text.

The square of correlation was slightly, but non-significantly (p = 0.16), higher when it was allowed to go to its naturally chosen Ymax of 78% than when it was forced the fit through 100% (Fig 3.12 and Table 3.8). This indicates that there might have been an actual total recovery. The averaged figures (Table 3.7) and not the pooled data (Table 3.8) will be used in the discussion.

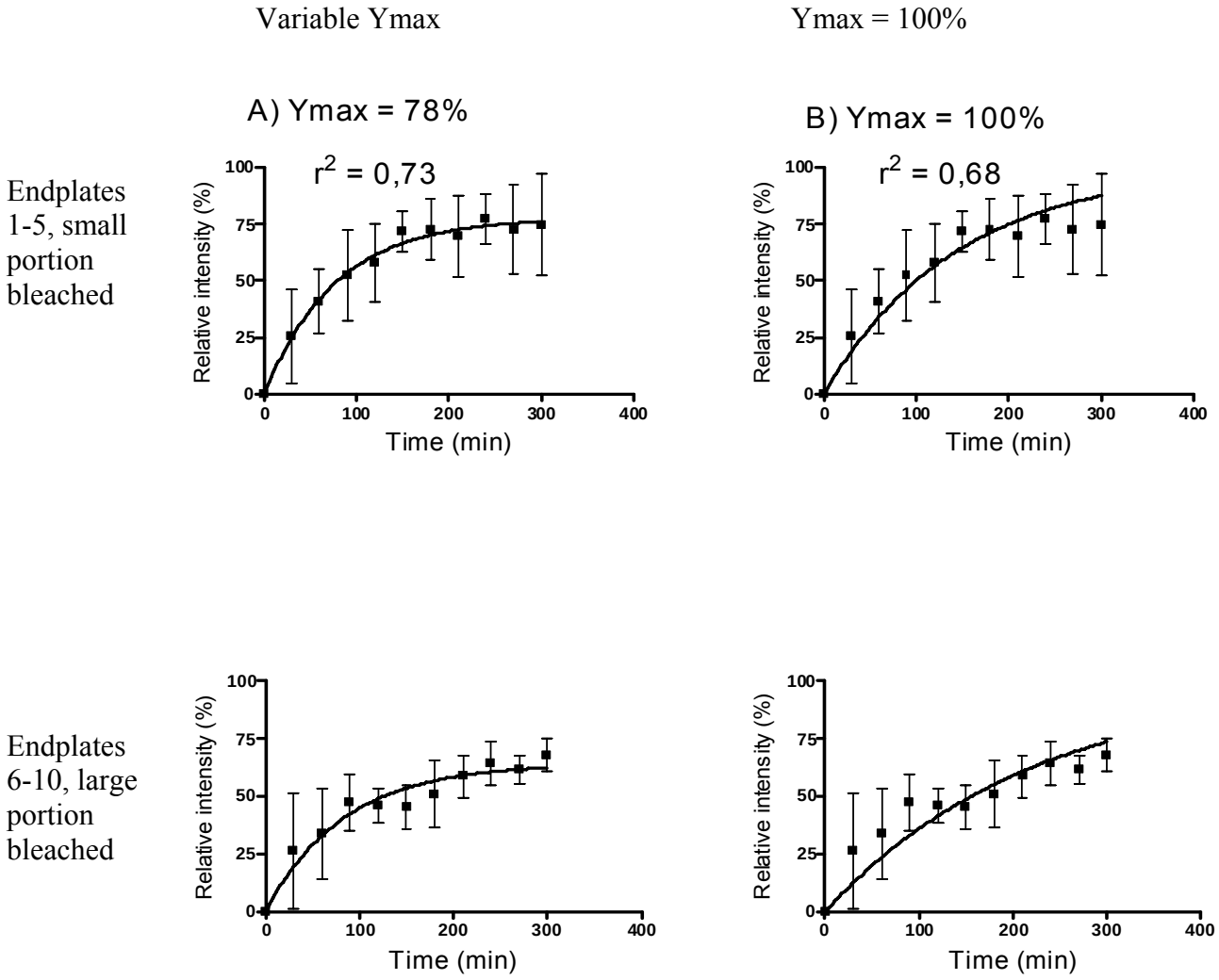

Figure 3.12 Total recovery of endplates 1-5 and 6-10. Recovery of each endplate is found by adding the decrease in relative intensity at each time point for the same endplate. The data is fitted to one phase exponentials both with and without constraints. Endplates 1-5 with Ymax = 78% A), and an Ymax set to 100% B). Endplates 6-10 with an Ymax of 64% C), and Ymax set to 100% D. Endplate 8 is excluded as done in all analysis concerning measurements outside the bleached area of the endplates.

Graph	Pooled from endplates	Ymax ± SEM (%)	$t_{1/2}$ 1 (min)	r^2
A	1-5	77.83 ± 4.814	53.69	0.7279
B	1-5	100	100.1	0.6765
C	6,7,9 and 10	64.28 ± 4.607	57.91	0.6999
D	6,7,9 and 10	100.0	155.4	0.6179

Table 3.8 Data of total recovery graphs. A-D corresponds to the graphs in Fig. 3.12. Maximal recovery obtained with the graph fit (Ymax), the half recovery time ($t_{1/2}$**)** and the square of correlation (r^2) values are listed. For Ymax values standard error of mean (SEM) is shown. For graph B and D Ymax was set to 100% and therefore has no standard error.

4 DISCUSSION

Previous evidence indicates that rapsyn and the AChR move around in the muscle fibre as a complex. Wang et al. (1999) suggested that AChRs are associated with rapsyn both in clusters and outside of these. In support of this Gervasio and Phillips (2005) have showen that the two proteins have the same recovery rate after photobleaching in C2 myotubes, both in the diffuse and in the clustered state. They propose that the two proteins exist as a stable protein complex both before and after clustering. The aim of this study was to investigate whether rapsyn had the same recovery rate after photobleaching as the receptor. Contrary to what we expect we found that rapsyn had a faster recovery rate after bleaching in vivo than established for the AChR.

4.1 Three sources of unbleached rapsyn-EGFP

There are three possible sources within the fibre from which the bleached endplate area can retrieve unbleached molecules: (1) the unbleached portion of the same endplate, (2) the surrounding plasma membrane and (3) the intracellular pool, which consists of (a) the cytosol, (b) the golgi network and other intracellular compartments, or new synthesis through any of these three sources (Fig. 4.1). The unbleached part of the endplate is a limited source, where the amount of molecules is directly proportional to the size of the unbleached endplate region. On the other hand the amount of rapsyn-EGFP in the intracellular compartments and the membrane remains uncertain, particularly upon overexpression.

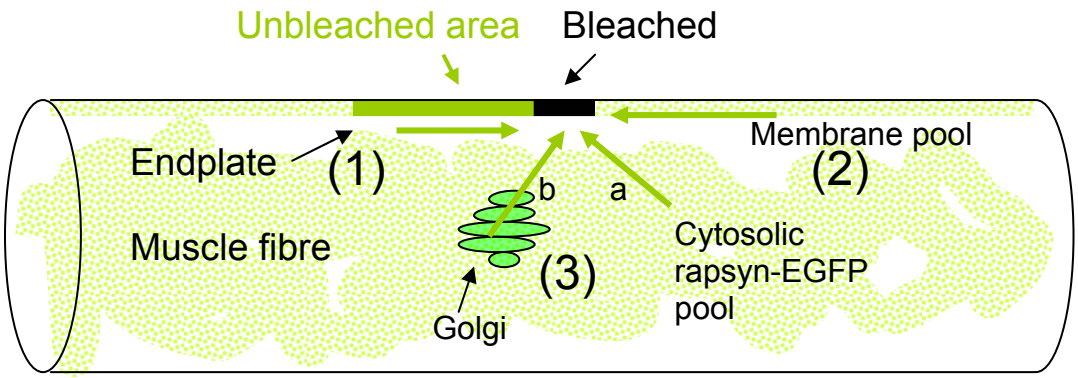

Figure 4.1 Schematic illustration of three possible sources of unbleached rapsyn-EGFP. A section of a muscle fibre is illustrated with the endplate filled with rapsyn-EGFP visible on the top (in green). The right part of the endplate has been bleached (shown in black). The three possible sources of unbleached rapsyn-EGFPs that can migrate to the bleached endplate area and lead to recovery here is; (1) the relatively limited supply of the unbleached part of the same endplate (2) the plasma membrane and (3) intracellular compartments and new synthesis.

The lateral mobility of AChRs through the membrane takes place both within the endplate and between the endplate and the perisynaptic membrane area (Akaaboune *et al.*, 2002). The receptor density in the endplate is kept high by introducing receptors from the surroundings (Akaaboune *et al.*, 2002). Rapsyn recovery is probably also supplied by more than one of these three pools (se below).

4.2 The unbleached part of the endplate is not sufficient to sustain the registered recovery

If the only source of unbleached molecules was within the same endplate and the rapsyn-EGFPs are distributed evenly over the endplate, the maximal recovery would be obtained when the bleached and unbleached molecules reached an equal distribution within the endplate, assuming random movement. This would give a recovery corresponding to the percentage of the unbleached molecules of the total endplate-population.

In the present material such a theoretical recovery would be 96% for the small bleached areas (endplates 1-5) and 22% for the large bleached areas (endplates 6-10). For endplates 1-5 this is not too far from the average recovery of 73% (Table 3.7). However, for endplates 6-10, which have a large portion bleached, the recovery of 68.1% was about three times larger than the possible theoretical recovery. This indicates that the migration of rapsyn-EGFP molecules from unbleached parts of the same endplate was probably not the main source. As previously described for the receptor (Akaaboune *et al.*, 2002), rapsyn-EGFP seems to move in from both the membrane surrounding the endplate and the cytosol in order to keep up a high density of molecules in the endplate.

4.3 Do all the rapsyn-EGFP molecules display the same recovery rate?

The recovery process that was observed, was a single exponential association (section 3.1.2 and 3.2.2). However, if the recovery curves of the bleached areas had an Ymax of less than 100% this would imply that the non-recovered portion of the molecules in the bleached area

was close to immobile, relative to the time range of these experiments. This would indicate two pools of rapsyn-EGFP molecules in the analysed endplates. The "slow portion" would have such a low recovery rate that it would not be evident within five hours.

For endplates which have a small portion bleached, the average Ymax was 73%, while for endplates which have a large portion bleached, average Ymax was 68%. These were both significantly different from 100% ($p = 0.01$), but not significantly different from each other ($p = 0.3$). This indicates a mobile pool constituting ~ 60-80% of the total amount of rapsyn-EGFP in the endplate with half recovery times ranging from 20-100min (Table 3.7). The rest, ~20-40% would have a much longer half-life. According to the data shown here, there were probably two pools of rapsyn, but to be certain one would have to redo the experiments and record the recovery over a longer time range.

4.4 Rapsyn has a faster recovery after photobleaching than the AChR

Akaaboune et al. (2002) subsaturated the AChR with α-BuT so that synaptic transmission remained functional. They then bleached the whole endplate down to 4.5% of the initial intensity. After two days, a recovery of 8% was registered (Akaaboune *et al.*, 2002). This gives 0.2% per hour. This is a much lower recovery rate than what we found in our experiments with rapsyn. When we bleached a large portion of endplates, the result was an average recovery of 68% after 5 hours, or 13.6% per hour (Table 3.7). This is a 68-fold difference. Even when the general decrease in intensity seen in all endplates is not considered, a total recovery of 12% or 2.45% per hour results (Fig. 3.9). This is a 12-fold higher recovery rate.

A large difference between our experiments and those of Akaaboune et al. (2002) is, however, that they bleached the entire endplate while we bleached a part of it (about 79% for endplate 6-10). As a result of bleaching the entire endplate there would be no source of supplying molecules within the same endplate. Still, as discussed previously this endplate pool did not seem to play a major role in our registered recovery. It is unlikely that our recovery would be

reduced down 12-68-fold if the entire endplate were bleached. Why then is the recovery of rapsyn faster than that found for the receptor?

4.4.1 Photo-unbinding is unlikely the reason for the quick recovery measured

Akaaboune et al. (2002) propose that the process of photo-unbinding (described in section 2.5) can influence the recovery rate of AChR. It is unlikely, however that this process can account for the faster recorded recovery of rapsyn-EGFP. Unbinding is approximately proportional to the square of the light intensity and with high intensity, such as used here and in Akaaboune et al. (2002)'s study, up to 14% of the α-BuT will undergo photo-unbinding from the receptor instead of bleaching (Akaaboune *et al.*, 2002).

Unlike the AChR, which is tagged with the small, fluorescently marked α-BuT that can dissociate from the receptor, Rapsyn-EGFP is a fusion protein, which by itself is fluorescent. It is unlikely that the laser should cause the protein to split. Nevertheless, it might be possible that the high laser light intensity could result in rapsyn-EGFP dissociating from the receptor and thereby increasing the mobility of a portion of the rapsyn-EGFP. On the other hand Rapsyn-EGFP is a much larger protein (72kD) than the small α-BuT (8kD). The process if possible, is therefore likely to require an even higher intensity of light. There is also no significant recovery observed upon bleaching clustered rapsyn-EGFP or in fixed cells (Gervasio & Phillips, 2005).

4.4.2 Do rapsyn molecules bind and dissociate from AChR?

The data presented here, can be explained in two ways, depending on whether there were in fact one or two pools of rapsyn-EGFP in the endplate. If we assume there was only one population, all of the rapsyn-EGFP molecules have a much faster recovery after photobleaching than the receptor. This would indicate that rapsyn and the receptor cannot act as a stable complex and that rapsyn-EGFP is free from the receptor and has a faster mobility and/or turnover. A faster turnover of rapsyn-EGFP than of the AChR is consistent with the

fact that in cell culture, rapsyn has a turnover of about three times faster than the receptor (Frail *et al.*, 1989).

However, according to the data presented here, there seemed to be two pools of rapsyn-EGFP in the endplate – one pool with a high recovery rate, and one with such a low rate that they did not contribute to the measured recovery. These consisted of 60-80% (Table 3.8) and 20-40% of the endplate population respectively. For the large mobile pool, two possibilities exist, either the rapsyn-EGFP is free from the receptor and moves in the muscle membrane independently of these, or rapsyn-EGFP is associated with the receptor for shorter time periods. The small non-recovered pool of rapsyn-EGFP might possibly be bound in stable complexes with receptors (Fig. 4.2), which will be discussed below.

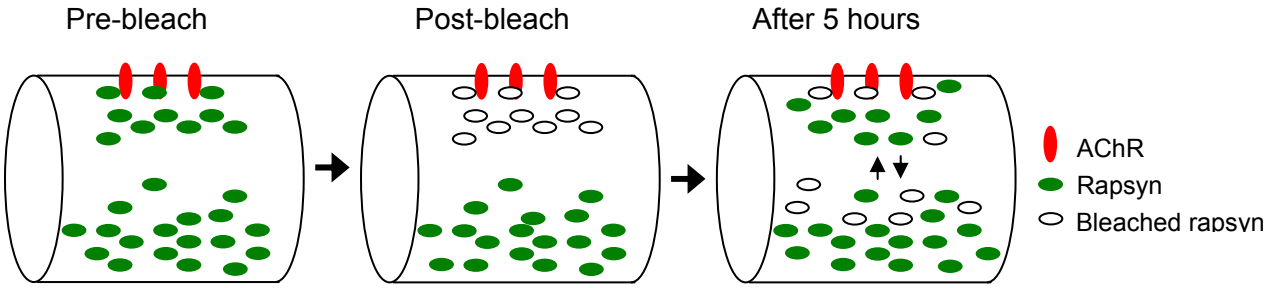

Figure 4.2 Model of rapsyn mobility. There are possibly two pools of rapsyn- (green structures) EGFP in the endplate, one associated tightly with the AChR (red) constituting 20-40% of the endplate population and one free or loosely associated population of 60-80%. This fast recovering population moves around more freely in the muscle fibre and most will have recovered within the five hours. While the AChR associated rapsyn-EGFP molecules are not free to move around and no recovery is seen for this population.

What then, is the basis of these two pools? The amount of rapsyn-EGFP in the endplate is close to doubled upon overexpression of the molecule (Gervasio & Phillips, 2005). Possibly, overexpression of rapsyn-EGFP leads to two pools. The amount of rapsyn normally associated with receptors in the endplate would constitute the pool of rapsyn with no visible recovery during the five hours. The additional amount of rapsyn-EGFP introduced into the endplate upon overexpression constitutes the pool of 60-80% giving the high recovery. However, if this is the case, the mobile pool should be slightly smaller than the receptor bound pool. Then again, about 75% of the wild type rapsyn is still left in the endplate (Gervasio & Phillips, 2005). Assuming the already present wild type rapsyn is part of the

receptor bound pool, this pool contains about 95-115% while the quick recovering pool consist of about 60-80%, corresponding well with the 1.8 times increase in rapsyn density in the endplate.

If overexpression is the foundation for the two pools, it is possible to think that the non-recovered pool was tightly associated with receptors while the recovered portion was not. However, all rapsyn-EGFP in the endplate must be associated with specific endplate components in some way to have an increase in density here. Rapsyn self-association and β-dystroglycan are both possible candidates for this.

Several factors indicate that also the fast recovered pool of rapsyn-EGFP is associated with receptors at the endplate. The linear relationship found between rapsyn-EGFP and TRITC-α-BuT intensities in endplates, upon overexpression of rapsyn-EGFP, implies that rapsyn-EGFP binds either directly to AChRs, or to some other molecule that is in strict proportion to the AChR (Gervasio & Phillips, 2005). Secondly, overexpression of rapsyn-EGFP in the endplate leads to a stabilisation of AChR in the endplate, indicating that all rapsyns are in some way associated with receptors at the endplate. However, for rapsyn-EGFP to be able to have a faster recovery than the receptor it cannot act as a stable complex with the receptor. Still, it is possible, that rapsyn-EGFP binds and dissociates from the receptor at a higher or lower rate and that they act as complexes for shorter time periods.

As mentioned above, the receptor has a half recovery time of about 0.2% per hour. This would amount to 1% after 5 hours. If the receptor bound fraction of rapsyn-EGFP, constituting 20-40%, recovered at this low rate it would not be possible to discriminate this recovery from the large recovery of the mobile fraction. It is therefore possible to think that this pool of rapsyn-EGFP act as a stable complex with the AChR.

A combination of the two main scenarios is also possible, that is, a faster turnover of all molecules and two populations with different degrees of receptor binding. Even with two pools of rapsyn-EGFP in the endplate it is probable that all of the molecules have a higher rate of turnover than the receptor, as found in cell culture (Frail *et al.*, 1989). The less mobile pool of rapsyn-EGFP, could be bound to AChR throughout its shorter lifetime or possibly for

shorter or longer time periods. At the same time, the non-recovered portion could be associated with receptors for even shorter periods of time, or not at all.

4.5 Conclusion

On the basis of our experiment it seems possible, on the basis of their recovery rate, to divide Rapsyn-EGFP in muscle endplates into two pools. The first of these pools has a much faster recovery after photobleaching than shown earlier for AChRs, indicating a faster turnover and mobility than the receptor. These may either be independent of receptors or they may bind and dissociate from them and act as complexes with them during shorter time periods. The second pool consisting of non-recovered molecules, however, can possibly exist as stable complexes with AChR during the shorter lifetime of the rapsyn-EGFP molecule.

As shown for the receptor, rapsyn seem to move laterally within the endplate and rapsyn molecules also migrate into the endplate from the surrounding area. To get a clearer picture of the relationship between rapsyn and the receptor, one would need to do double FRAP experiments on endplates by tagging AChR with α-BuT after rapsyn-EGFP electroporation followed by simultaneous bleaching of both rapsyn-EGFP and AchR. One would than need to follow the endplates over a longer time span, corresponding to the longer half recovery time of the receptor.

APPENDIX A: ABBREVIATIONS

α-BuT	α-Bungarotoxin
ACh	Acetylcholine
AChE	Acetylcholine estrase
AChR	Acetylcholine receptor
ATP	Adenosine triphosphate
cDNA	complementary Deoxyribonucleic Acid
CMV	Cytomegalovirus Immediate early gene
DGC	Dystrophin-glycoprotein complex
DNA	Deoxyribonucleic Acid
edl	*extensor digitorum longu*
EGFP	Enhanced Green Fluorescent Protein
EP	Endplate
FPR	Fluorescence Photobleaching Recovery
FRAP	Fluorescent Recovery After Photobleaching
MuSK	Muscle Specific Kinase
p.v.	Pixel values
r^2	square of correlation
Rapsyn	Receptor Associated Protein at the SYNnapse
SEM	Standard Error of Mean
SD	Standard Deviation
SIT	Silicon Intensified Tube
$t_{1/2}$	Half recovery time
TPRs	Tetracopeptide Repeats
TTX	Tertrodotoxin
Ymax	Maximal recovery
wt	Wild type

APPENDIX B: PROTOCOLS

Equthesin (catalognumber 702821, Ullevål pharmacy)

Chloral hydrate	42.5 mg
Magnesium sulphate	21.0 mg
Pentobarbitone	9.7 mg
Ethanol (96%)	76 mg
Propylenglycol	428 mg
dH_2O	50 ml

DNA solution for electroporation (100 µl)

DNA plasmid in H_2O (2 µg/µl)	50 µl
NaCl (4M)	4 µl
dH_2O	46 µl

Ringer lactate (1000 ml)

NaCl	6 g
Potasiumchloride	300 mg
Calciumchloride dihydrate	200 mg
Sodiumlactate	3.1 g
dH_2O	1000 ml

REFERENCES

AKAABOUNE, M., CULICAN, S. M., TURNEY, S. G. & LICHTMAN, J. W. (1999). Rapid and reversible effects of activity on acetylcholine receptor density at the neuromuscular junction in vivo. *Science* **286,** 503-507.

AKAABOUNE, M., GRADY, R. M., TURNEY, S., SANES, J. R. & LICHTMAN, J. W. (2002). Neurotransmitter receptor dynamics studied in vivo by reversible photo-unbinding of fluorescent ligands. *Neuron* **34,** 865-876.

ANDERSON, M. J. & COHEN, M. W. (1977). Nerve-induced and spontaneous redistribution of acetylcholine receptors on cultured muscle cells. *J Physiol* **268,** 757-773.

APEL, E. D., ROBERDS, S. L., CAMPBELL, K. P. & MERLIE, J. P. (1995). Rapsyn may function as a link between the acetylcholine receptor and the agrin-binding dystrophin-associated glycoprotein complex. *Neuron* **15,** 115-126.

AXELROD, D., KOPPEL, D. E., SCHLESSINGER, J., ELSON, E. L. & WEBB, W. W. (1976a). Mobility measurment by analysis of fluorescence photobleaching recovery kinetics. *Biophysical journal* **16,** 1055-1069.

AXELROD, D., RAVDIN, P., KOPPEL, D. E., SCHLESSINGER, J., WEBB, W. W., ELSON, E. L. & PODLESKI, T. R. (1976b). Lateral motion of fluorescently labeled acetylcholine receptors in membranes of developing muscle fibers. *Proc Natl Acad Sci U S A* **73,** 4594-4598.

BARRANTES, F. J., NEUGEBAUER, D.-C. & ZINGSHEIM, H. P. (1980). Peptide extraction by alkaline treatment is accompanied by rearrangement of the membra-bound acetylcholine receptor from Torpedo marmorate. *FEBS Lett* **112,** 73-78.

BARTOLI, M., RAMARAO, M. K. & COHEN, J. B. (2001). Interactions of the rapsyn RING-H2 domain with dystroglycan. *J Biol Chem* **276,** 24911-24917.

BERG, D. K. & HALL, Z. W. (1974). Fate of alpha-bungarotoxin bound to acetylcholine receptors of normal and denervated muscle. *Science* **184,** 473-475.

BLOCH, R. J. & HALL, Z. W. (1983). Cytoskeletal components of the vertebrate neuromuscular junction: vinculin, alpha-actinin, and filamin. *J Cell Biol* **97,** 217-223.

BURDEN, S. J., DEPALMA, R. L. & GOTTESMAN, G. S. (1983). Crosslinking of proteins in acetylcholine receptor-rich membranes: association between the beta-subunit and the 43 kd subsynaptic protein. *Cell* **35,** 687-692.

CARRERO, G., D., M., E., C., G., D. V. & J., H. M. (2003). Using FRAP and mathematical modeling to determine the in vivo kinetics of nuclear proteins. *ScienceDirect* **29,** 14-28.

COWAN, M. W., SUDHOF, T. C. & STEVENS, C. F. (2001). Synapses. In *The John Hopkins University Press*.

EDIDIN, M., ZAGYANSKY, Y. & LARDNER, T. J. (1976). Measurement of membrane protein lateral diffusion in single cells. *Science* **191,** 466-468.

FRAIL, D. E., MCLAUGHLIN, L. L., MUDD, J. & MERLIE, J. P. (1988). Identification of the mouse muscle 43,000-dalton acetylcholine receptor-associated protein (RAPsyn) by cDNA cloning. *J Biol Chem* **263,** 15602-15607.

FRAIL, D. E., MUDD, J., SHAH, V., CARR, C., COHEN, J. B. & MERLIE, J. P. (1987). cDNAs for the postsynaptic 43-kDa protein of Torpedo electric organ encode two proteins with different carboxyl termini. *Proc Natl Acad Sci U S A* **84,** 6302-6306.

FRAIL, D. E., MUSIL, L. S., BUONANNO, A., MERLIE, J. P., MCLAUGHLIN, L. L. & MUDD, J. (1989). Expression of RAPsyn (43K protein) and nicotinic acetylcholine receptor genes is not coordinately regulated in mouse muscle
Identification of the mouse muscle 43,000-dalton acetylcholine receptor-associated protein (RAPsyn) by cDNA cloning. *Neuron* **2,** 1077-1086.

FREEMONT, P. S. (1993). The RING finger. A novel protein sequence motif related to the zinc finger. *Ann N Y Acad Sci* **684,** 174-192.

FROEHNER, S. C., GULBRANDSEN, V., HYMAN, C., JENG, A. Y., NEUBIG, R. R. & COHEN, J. B. (1981). Immunofluorescence localization at the mammalian neuromuscular junction of the Mr 43,000 protein of Torpedo postsynaptic membranes. *Proc Natl Acad Sci U S A* **78,** 5230-5234.

FROEHNER, S. C., LUETJE, C. W., SCOTLAND, P. B. & PATRICK, J. (1990). The postsynaptic 43K protein clusters muscle nicotinic acetylcholine receptors in Xenopus oocytes. *Neuron* **5,** 403-410.

GAUTAM, M., NOAKES, P. G., MUDD, J., NICHOL, M., CHU, G. C., SANES, J. R. & MERLIE, J. P. (1995). Failure of postsynaptic specialization to develop at neuromuscular junctions of rapsyn-deficient mice. *Nature* **377,** 232-236.

GERVASIO, O. L. & PHILLIPS, W. D. (2005). Increased ratio of rapsyn to ACh receptor stabilizes postsynaptic receptors at the mouse neuromuscular synapse. *J Physiol* **562,** 673-685. Epub 2004 Nov 2018.

GILLESPIE, S. K., BALASUBRAMANIAN, S., FUNG, E. T. & HUGANIR, R. L. (1996). Rapsyn clusters and activates the synapse-specific receptor tyrosine kinase MuSK. *Neuron* **16,** 953-962.

HALL, Z. W. & SANES, J. R. (1993). Synaptic structure and development: the neuromuscular junction. *Cell* **72 Suppl,** 99-121.

HEUSER, J. E. & SALPETER, S. R. (1979). Organization of acetylcholine receptors in quick-frozen, deep-etched, and rotary-replicated Torpedo postsynaptic membrane. *J Cell Biol* **82,** 150-173.

HIROKAWA, N. & HEUSER, J. E. (1982). Internal and external differentiations of the postsynaptic membrane at the neuromuscular junction. *J Neurocytol* **11,** 487-510.

HUEBSCH, K. A. & MAIMONE, M. M. (2003). Rapsyn-mediated clustering of acetylcholine receptor subunits requires the major cytoplasmic loop of the receptor subunits. *J Neurobiol* **54,** 486-501.

JACOBSON, K., DERZKO, Z., WU, E. S., HOU, Y. & POSTE, G. (1976). Measurement of the lateral mobility of cell surface components in single, living cells by fluorescence recovery after photobleaching. *J Supramol Struct* **5,** 565(417)-576(428).

KUROMI, H., BRASS, B. & KIDOKORO, Y. (1985). Formation of acetylcholine receptor clusters at neuromuscular junction in Xenopus cultures. *Dev Biol* **109,** 165-176.

LAROCHELLE, W. J. & FROEHNER, S. C. (1986). Determination of the tissue distributions and relative concentrations of the postsynaptic 43-kDa protein and the acetylcholine receptor in Torpedo. *J Biol Chem* **261,** 5270-5274.

MAIMONE, M. M. & MERLIE, J. P. (1993). Interaction of the 43 kd postsynaptic protein with all subunits of the muscle nicotinic acetylcholine receptor. *Neuron* **11,** 53-66.

MARCHAND, S., DEVILLERS-THIERY, A., PONS, S., CHANGEUX, J. P. & CARTAUD, J. (2002). Rapsyn escorts the nicotinic acetylcholine receptor along the exocytic pathway via association with lipid rafts. *J Neurosci* **22,** 8891-8901.

MATHIESEN, I. (1999). Electropermeabilization of skeletal muscle enhances gene transfer in vivo. *Gene Ther* **6,** 508-514.

MIYAZAWA, A., FUJIYOSHI, Y., STOWELL, M. & UNWIN, N. (1999). Nicotinic acetylcholine receptor at 4.6 A resolution: transverse tunnels in the channel wall. *J Mol Biol* **288,** 765-786.

MOHAMED, A. S. & SWOPE, S. L. (1999). Phosphorylation and cytoskeletal anchoring of the acetylcholine receptor by Src class protein-tyrosine kinases. Activation by rapsyn. *J Biol Chem* **274,** 20529-20539.

NEUBIG, R. R., KRODEL, E. K., BOYD, N. D. & COHEN, J. B. (1979). Acetylcholine and local anesthetic binding to Torpedo nicotinic postsynaptic membranes after removal of nonreceptor peptides. *Proc Natl Acad Sci U S A* **76,** 690-694.

PENG, H. B. (1983). Cytoskeletal organization of the presynaptic nerve terminal and the acetylcholine receptor cluster in cell cultures. *J Cell Biol* **97,** 489-498.

PENG, H. B., ZHAO, D. Y., XIE, M. Z., SHEN, Z. W. & JACOBSON, K. (1989). The role of lateral migration in the formation of acetylcholine receptor clusters induced by basic polypeptide-coated latex beads. *Dev Biol* **131,** 197-206.

PHILLIPS, W. D., KOPTA, C., BLOUNT, P., GARDNER, P. D., STEINBACH, J. H. & MERLIE, J. P. (1991a). ACh receptor-rich membrane domains organized in fibroblasts by recombinant 43-kildalton protein. *Science* **251,** 568-570.

PHILLIPS, W. D., MAIMONE, M. M. & MERLIE, J. P. (1991b). Mutagenesis of the 43-kD postsynaptic protein defines domains involved in plasma membrane targeting and AChR clustering. *J Cell Biol* **115,** 1713-1723.

PHILLIPS, W. D., NOAKES, P. G., ROBERDS, S. L., CAMPBELL, K. P. & MERLIE, J. P. (1993). Clustering and immobilization of acetylcholine receptors by the 43-kD protein: a possible role for dystrophin-related protein. *J Cell Biol* **123,** 729-740.

PHILLIPS, W. D., VLADETA, D., HAN, H. & NOAKES, P. G. (1997). Rapsyn and agrin slow the metabolic degradation of the acetylcholine receptor. *Mol Cell Neurosci* **10,** 16-26.

PONTING, C. C. & PHILLIPS, C. (1996). Rapsyn's knobs and holes: eight tetratrico peptide repeats. *Biochem J* **314 (Pt 3),** 1053-1054.

PORTER, S. & FROEHNER, S. C. (1983). Characterization and localization of the Mr = 43,000 proteins associated with acetylcholine receptor-rich membranes. *J Biol Chem* **258,** 10034-10040.

RAMARAO, M. K., BIANCHETTA, M. J., LANKEN, J. & COHEN, J. B. (2001). Role of rapsyn tetratricopeptide repeat and coiled-coil domains in self-association and nicotinic acetylcholine receptor clustering. *J Biol Chem* **276,** 7475-7483.

RAMARAO, M. K. & COHEN, J. B. (1998). Mechanism of nicotinic acetylcholine receptor cluster formation by rapsyn. *Proc Natl Acad Sci U S A* **95,** 4007-4012.

RANA, Z. A., GUNDERSEN, K., BUONANNO, A. & VULLHORST, D. (2005). Imaging transcription in vivo: distinct regulatory effects of fast and slow activity patterns on promoter elements from vertebrate troponin I isoform genes. *J Physiol* **562,** 815-828.

ROUSSELET, A., CARTAUD, J., DEVAUX, P. F. & CHANGEUX, J. P. (1982). The rotational diffusion of the acetylcholine receptor in Torpeda marmorata membrane fragments studied with a spin-labelled alpha-toxin: importance of the 43 000 protein(s). *Embo J* **1,** 439-445.

RUEGG, M. A. & BIXBY, J. L. (1998). Agrin orchestrates synaptic differentiation at the vertebrate neuromuscular junction. *Trends Neurosci* **21,** 22-27.

SAITOH, T., WENNOGLE, L. P. & CHANGEUX, J. P. (1979). Factors regulating the susceptibility of the acetylcholine receptor protein to heat inactivation. *FEBS Lett* **108,** 489-494.

SANDER, A., HESSER, B. A. & WITZEMANN, V. (2001). MuSK induces in vivo acetylcholine receptor clusters in a ligand-independent manner. *J Cell Biol* **155,** 1287-1296.

SANES, J. R. & LICHTMAN, J. W. (1999). Development of the vertebrate neuromuscular junction. *Annu Rev Neurosci* **22,** 389-442.

SCHLESSINGER, J., KOPPEL, D. E., AXELROD, D., JACOBSON, K., WEBB, W. W. & ELSON, E. L. (1976). Lateral transport on cell membranes: mobility of concanavalin A receptors on myoblasts. *Proc Natl Acad Sci U S A* **73,** 2409-2413.

SEALOCK, R. (1982). Cytoplasmic surface structure in postsynaptic membranes from electric tissue visualized by tannic-acid-mediated negative contrasting. *J Cell Biol* **92,** 514-522.

SOBEL, A. & CHANGEUX, J. P. (1977). Purification and characterization of the cholinergic receptor protein in its membrane-bound and detergent-soluble forms from the electric organ of Torpedo marmorata. *Biochem Soc Trans* **5,** 511-514.

SOBEL, A., HEIDMANN, T. & CHANGEUX, J. P. (1977a). [Purification of a protein binding quinacrine and histrionicotoxin from membrane fragments rich in cholinergic receptors in Torpedo marmorata]. *C R Acad Sci Hebd Seances Acad Sci D* **285,** 1255-1258.

SOBEL, A., HEIDMANN, T., HOFLER, J. & CHANGEUX, J. P. (1978). Distinct protein components from Torpedo marmorata membranes carry the acetylcholine receptor site and the binding site for local anesthetics and histrionicotoxin. *Proc Natl Acad Sci U S A* **75,** 510-514.

SOBEL, A., WEBER, M. & CHANGEUX, J. P. (1977b). Large-scale purification of the acetylcholine-receptor protein in its membrane-bound and detergent-extracted forms from Torpedo marmorata electric organ. *Eur J Biochem* **80,** 215-224.

ST JOHN, P. A., FROEHNER, S. C., GOODENOUGH, D. A. & COHEN, J. B. (1982). Nicotinic postsynaptic membranes from Torpedo: sidedness, permeability to macromolecules, and topography of major polypeptides. *J Cell Biol* **92,** 333-342.

STEINBACH, J. H., MERLIE, J., HEINEMANN, S. & BLOCH, R. (1979). Degradation of junctional and extrajunctional acetylcholine receptors by developing rat skeletal muscle. *Proc Natl Acad Sci U S A* **76,** 3547-3551.

STYA, M. & AXELROD, D. (1983). Mobility and detergent extractability of acetylcholine receptors on cultured rat myotubes: a correlation. *J Cell Biol* **97,** 48-51.

STYA, M. & AXELROD, D. (1984). Mobility of extrajunctional acetylcholine receptors on denervated adult muscle fibers. *J Neurosci* **4,** 70-74.

VELEZ, M., BARALD, K. F. & AXELROD, D. (1990). Rotational diffusion of acetylcholine receptors on cultured rat myotubes. *J Cell Biol* **110,** 2049-2059.

WANG, Z. Z., MATHIAS, A., GAUTAM, M. & HALL, Z. W. (1999). Metabolic stabilization of muscle nicotinic acetylcholine receptor by rapsyn. *J Neurosci* **19,** 1998-2007.

WENNOGLE, L. P. & CHANGEUX, J. P. (1980). Transmembrane orientation of proteins present in acetylcholine receptor-rich membranes from Torpedo marmorata studied by selective proteolysis. *Eur J Biochem* **106,** 381-393.

WOLFF, J. A., MALONE, R. W., WILLIAMS, P., CHONG, W., ACSADI, G., JANI, A. & FELGNER, P. L. (1990). Direct gene transfer into mouse muscle in vivo. *Science* **247,** 1465-1468.

ZAGYANSKY, Y. & EDIDIN, M. (1976). Lateral diffusion of concanavalin A receptors in the plasma membrane of mouse fibroblasts. *Biochim Biophys Acta* **433,** 209-214.